Contrib Mineral Petrol (2006) 151: 121–140
DOI 10.1007/s00410-005-0060-5

ORIGINAL PAPER

V. J. E. Buckley · R. S. J. Sparks · B. J. Wood

Hornblende dehydration reactions during magma ascent at Soufrière Hills Volcano, Montserrat

Received: 7 February 2005 / Accepted: 9 December 2005 / Published online: 13 January 2006

Abstract Hornblende phenocrysts in recent andesites of the Soufrière Hills Volcano display reaction rims of microcrystalline plagioclase, pyroxene, Fe-oxides and interstitial glass, formed by decompression during magma ascent. Mass balance calculations give the following reactions with mineral proportions in agreement with modal abundances:

100.0hbl→49.8cpx+27.6opx+18.2plag+4.5Ti-mag
100.0hbl→53.9cpx+24.4opx+18.1plag+1.9ilm+1.7mag

These reactions require an open chemical system with exchange of selected components with surrounding melt. Volatiles, TiO_2 and alkalis are expelled and SiO_2 and FeO^T are consumed. Matrix glasses fall into two compositional groups. Glasses in pumice are relatively rich in CaO and poor in K_2O and Na_2O compared to glasses in dome samples. The former glasses formed by moderate amounts of groundmass crystallisation of plagioclase, associated with rapid magma ascent in explosive eruptions. The later glasses evolved in response to hornblende breakdown, groundmass crystallisation and mixing of melts from different levels during slow magma ascent and extended residence time in the dome. Interstitial glass compositions in reaction rims reflect the compositions of the surrounding matrix glasses, but show variable compositional differences mostly consistent with the proposed open-system reactions.

Introduction

Hornblende phenocrysts are abundant in volatile-rich orogenic andesites. Many display breakdown textures, including reaction rims of microcrystalline plagioclase, pyroxene and Fe-oxides, forming microcrystalline rims enveloping remnant hornblende cores. This texture can develop during magma ascent and decompression as hornblende becomes unstable in the presence of coexisting melt with decreasing dissolved water content. Reaction rim width is dependent on the over-steps in temperature and pressure. It is also a function of decompression rate; consequently, the potential exists to estimate magma ascent rates from rim width measurements (Rutherford and Hill 1993).

In a pioneering experimental study Rutherford and Hill (1993) measured hornblende reaction rim width as a function of time for the Mount St. Helens (MSH) May 18, 1980, dacite. They then estimated magma ascent rates for the eruption by applying this calibration to interpret reaction rim width data from natural samples. Strictly this method is only directly applicable to the specific conditions of the experimental calibration for the MSH compositions and magma ascent rates obtained for other eruptions by extrapolation outside these conditions may not be quantitatively accurate. More general application of this technique therefore requires an understanding of the kinetic controls on the rates of hornblende dehydration reactions.

One important question concerns the nature and extent of material transport during the reaction, as different elements or species are likely to diffuse at different rates. Does amphibole breakdown in a semi-closed system involve near-isochemical conversion of amphibole to the anhydrous products with the release of volatiles, or does the reaction take place in an open chemical system with diffusive exchanges of chemical components with the surrounding melt? These questions can be addressed by detailed assessment of the material balance between reactants and products.

Melt inclusions in hornblende, matrix glasses in the groundmass and glasses trapped within hornblende reaction rims may offer insights into the evolution of hornblende, and the reaction mechanism of hornblende breakdown. Hornblende reaction during decompression

Communicated by J. Hoefs

V. J. E. Buckley (✉) · R. S. J. Sparks · B. J. Wood
Department of Earth Sciences, University of Bristol, Wills Memorial Building, Queens Road, Bristol BS8 1RJ, UK
E-mail: steve.sparks@bristol.ac.uk
Tel.: +44-117-9545419
Fax: +44-117-9253385

may not be isochemical. Thus, variations of glass chemistry in reaction rims and adjacent areas of the matrix might reflect modifications related to the hornblende breakdown reaction.

We present new compositional data and material balance estimates for hornblende breakdown in andesite from the ongoing eruption of the Soufrière Hills Volcano, Montserrat. We also re-evaluate existing mass balance data for the 1980 eruptions of MSH (Rutherford and Hill 1993). Quantitative accounts of the extent of chemical exchange between hornblendes and their surroundings are established, forming the foundation for quantitative evaluation of the rates of material transport during hornblende dehydration reactions.

Previous work

Amphibole reaction textures have long been recognised and are commonly mentioned in petrological descriptions of andesites (e.g. Williams 1942; Schmidt 1957; Jakes and White 1972; Gust and Johnson 1981; Reagan et al. 1987; Clynne 1999). Hornblende reaction textures from MSH 1980–1986 andesites (Scarfe and Fuji 1987; Rutherford and Hill 1993) and recent Soufrière Hills Volcano andesites (Murphy et al. 2000; Devine et al. 1998a, 1998b; Rutherford and Devine 2003) have received particular attention.

Rutherford and Hill (1993) investigated decompression-induced reaction rims on hornblendes in the post May 18, 1980, MSH andesite. Using hornblende and reaction rim phase compositions in a mass balance petrologic mixing programme (Wright and Doherty 1970) they found that no combination of the product phases in the reaction rim reproduces the reactant hornblende composition. Based on observations that rim growth proceeds inwards from the crystal margins, and that no breakdown occurs in the hornblende interiors, they proposed that, rather than breaking down isochemically, amphibole reacts with the surrounding rhyolitic melt. This conclusion is supported by the observation that there is no breakdown where hornblende is in contact with another crystalline phase. Their mass balance solution indicates that 73 parts amphibole react with 27 parts melt by weight to form the reaction products (orthopyroxene, clinopyroxene, plagioclase and ilmenite):

$$73\,\text{amph} + 27\,\text{melt} \rightarrow 29\,\text{opx} + 24\,\text{cpx} + 43\,\text{plag} + 3\,\text{ilm} \quad (1)$$

In the process the remaining melt becomes enriched in SiO_2, K_2O and Na_2O and depleted in Al_2O_3, FeO and CaO.

This result is problematic because, as shown by Rutherford and Hill (1993), no single combination of hornblende and melt can exactly reproduce the composition of the reaction rim products. Hornblende and the host melt each contain more K_2O than any of the MSH reaction rim phases, thus excess K_2O is an unavoidable by-product of hornblende breakdown. Most other components (SiO_2, TiO_2, Al_2O_3, Fe_2O_3, MnO, MgO, CaO and Na_2O) can only be balanced by reacting hornblende with a proportion of host melt; however, optimum solutions for each component require hornblende and melt to be combined in different proportions. Hornblende breakdown can be alternatively described by a reaction of the form amph $\rightarrow$ cpx + opx + plag + mag + ilm $\pm$ residuals, where residuals convey the compositional differences between hornblende and the best-fit combination of product phases. These differences are conceivably balanced by the surrounding melt. This perspective has a number of advantages. Firstly, melt is not included as a phase in mass balance calculations, so there is no requirement for all elements present in the melt to contribute to the reaction. Secondly, there is no requirement for the composition of the melt to remain fixed. Thirdly, magnetite is present in MSH hornblende reaction rims but absent from the best-fit solution for the reaction amph + melt $\rightarrow$ cpx + opx + plag + Fe-oxides (Rutherford and Hill 1993). If melt is removed from the equation magnetite is required in the solution. Considering these limitations we cannot know whether existing mass balance calculations accurately reflect material transport behaviour during MSH hornblende breakdown reactions. A more detailed investigation clarifying these issues is necessary as a basis for quantitative treatment of transport processes.

Geological setting

The 1995-to-present (August 2004) eruption of Soufrière Hills Volcano, Montserrat (WI) is the latest in a series of andesitic, dome-forming eruptions in a history dating from >170 ka (Roobol and Smith 1998; Harford et al. 2002). The current eruption is thought to have been triggered by injection of mafic magma into a pre-existing andesitic magma storage region, causing non-uniform reheating and remobilisation of the resident magma (Murphy et al. 1998; Devine et al. 1998a). Injection of hot basaltic magma and local heating of the andesite has continued periodically throughout the eruption (Couch et al. 2001; Devine et al. 2003), and essentially every sample of erupted magma shows evidence of some mingling of a hotter basaltic andesite with the pre-existing andesite (Murphy et al. 1998; Rutherford and Devine 2003). The rate of magma recharge into the chamber controls the eruption rate (Sparks et al. 1998). The current eruption has seen large fluctuations in magma discharge rate, with pauses and pulses in magmatic activity (Sparks et al. 1998; Robertson et al. 2000).

Petrological background

Andesite is the predominant eruption product throughout Montserrat's history. The lava is a coarse-grained,

porphyritic, crystal-rich hornblende–hypersthene andesite (58–61 wt% SiO_2) containing minor ubiquitous mafic inclusions of basaltic andesite (Murphy et al. 2000). The petrology and geochemistry of the andesite have been documented continuously throughout the eruption (Devine et al. 1998a, 2003; Murphy et al. 2000). No significant temporal variation has been observed in either first order petrological features or bulk magma chemistry, although banded lava is common, reflecting local differences in phenocryst proportions, crystallinity, grain size and vesicularity. The andesite contains phenocrysts and microphenocrysts of plagioclase (30–35 wt%), amphibole (6–10 wt%), orthopyroxene (2–5 wt%), titanomagnetite (2–4 wt%) and quartz (< 0.5 wt%). Clinopyroxene (< 0.5 wt%) occurs as microphenocrysts, and apatite and ilmenite are present in trace amounts. Disequilibrium features consistent with variable heating of the magma storage region are common. Plagioclase phenocrysts exhibit strongly resorbed sieve-textured zones and sodic cores mantled by calcic rims. Some orthopyroxene phenocrysts have Mg- and Ca-rich rims and quartz crystals are often resorbed and surrounded by clinopyroxene reaction rims. Hornblendes range from euhedral to those completely pseudomorphed by pyroxene–plagioclase-oxide intergrowths. All variants of texture and composition can be observed in a single thin section.

There is wide variation in groundmass textures. Pumice clasts are glassy with minor microlites of plagioclase and up to 35 wt% glass, whereas some dome samples have highly crystalline groundmass with as little as 5% glass, abundant plagioclase microlites, oxides, orthopyroxene and crystalline silica mainly in the form of cristobalite (Murphy et al. 2000; Harford et al. 2003).

Hornblende

Explosive pumice ejecta contain predominantly pristine, euhedral or slightly rounded amphibole phenocrysts that are vitreous and green-coloured (Fig. 1a). In more slowly erupted dome samples a range of reaction textures is preserved (Devine et al. 1998a; Murphy et al. 2000). Many crystals have experienced slight to extensive oxidation and are variably replaced at the rims and along cleavage planes by a very fine aggregate of minute (~1–10 μm) Fe-oxides and pyroxene (opacitisation, cf Garcia and Jacobson 1979; Murphy et al. 2000). These hornblendes appear dark brown and are often opaque (Fig. 1b).

Reaction rims are common, surrounding and partially replacing hornblende phenocrysts with fine-grained (~5–30 μm) intergrowths of clinopyroxene, orthopyroxene, plagioclase and Fe-oxides (Fig. 1c). Rims occur only on hornblende in contact with melt and rim growth proceeds inward from the crystal margins. In general reaction rims preserve the euhedral morphology of the precursor hornblende and are of uniform width around a given crystal. Multiple populations of hornblende phenocrysts with fine-grained reaction rims have been identified at SHV (Devine et al. 1998b). The main population (about 90%) display thin (~100 μm) reaction rims, while the remainder display thicker (~200–400 μm wide) reaction rims. These reaction rims form as a result of magma decompression either during magma ascent or during pre-eruptive shallow storage (Garcia and Jacobson 1979; Rutherford and Hill 1993; Rutherford and Devine 2003). Rim width is dependent on time and the magnitude of overstep in temperature and pressure, as well as decompression rate (Rutherford and Hill 1993). Thin-rimmed hornblendes are thought to have ascended rapidly from a deep source within the hornblende stability field, whereas thicker-rimmed hornblendes ascended more slowly. In slowly erupted samples a spectrum of rim widths is common. Qualitatively grain size in these rims increases with rim width. Similar observations were made on MSH samples by Rutherford and Hill (1993) who attribute rim width variability to conduit flow processes; thicker rimmed hornblendes are attributed to slower moving magma near the conduit walls, or possibly even erosion of magma emplaced in the earlier phase of eruption when mass eruption rates were much higher. They propose that the different batches of magma are then intimately mixed during ascent.

Resorbed hornblende phenocrysts and coarse-grained (~30–200 μm) hornblende reaction rims, mineralogically similar to those described above, are also present in SHV andesites (Fig. 1d). Similar textures described from subvolcanic andesites and basalts from the Sarroch District, SW Sardinia (Conte 1993) have been attributed to magma heating and high-temperature hornblende destabilisation. Any or all of the reaction textures described above may be preserved in close proximity within a single sample. Sometimes individual hornblende phenocrysts display multiple reaction textures. Commonly reaction rims are accompanied by opacitisation (Fig. 1c), presumably due to late-stage oxidation of hornblende cores surviving previous heating or decompression events (Murphy et al. 2000).

Analytical techniques

Sample selection

Polished thin sections from samples of recent Soufrière Hills andesite were selected from the Montserrat Volcano Observatory sub-collection held at the University of Bristol. The chosen suite (Table 1) contains samples derived from a range of eruptive conditions, including explosion-derived pumice and ballistic clasts (October 1997 to March 1999), and lava blocks from dome building episodes during periods of lower extrusion rate (January 1997 to February 2001). In samples containing fine-grained hornblende reaction rims, compositions of the reactant amphiboles and compositions and proportions of the product phases were

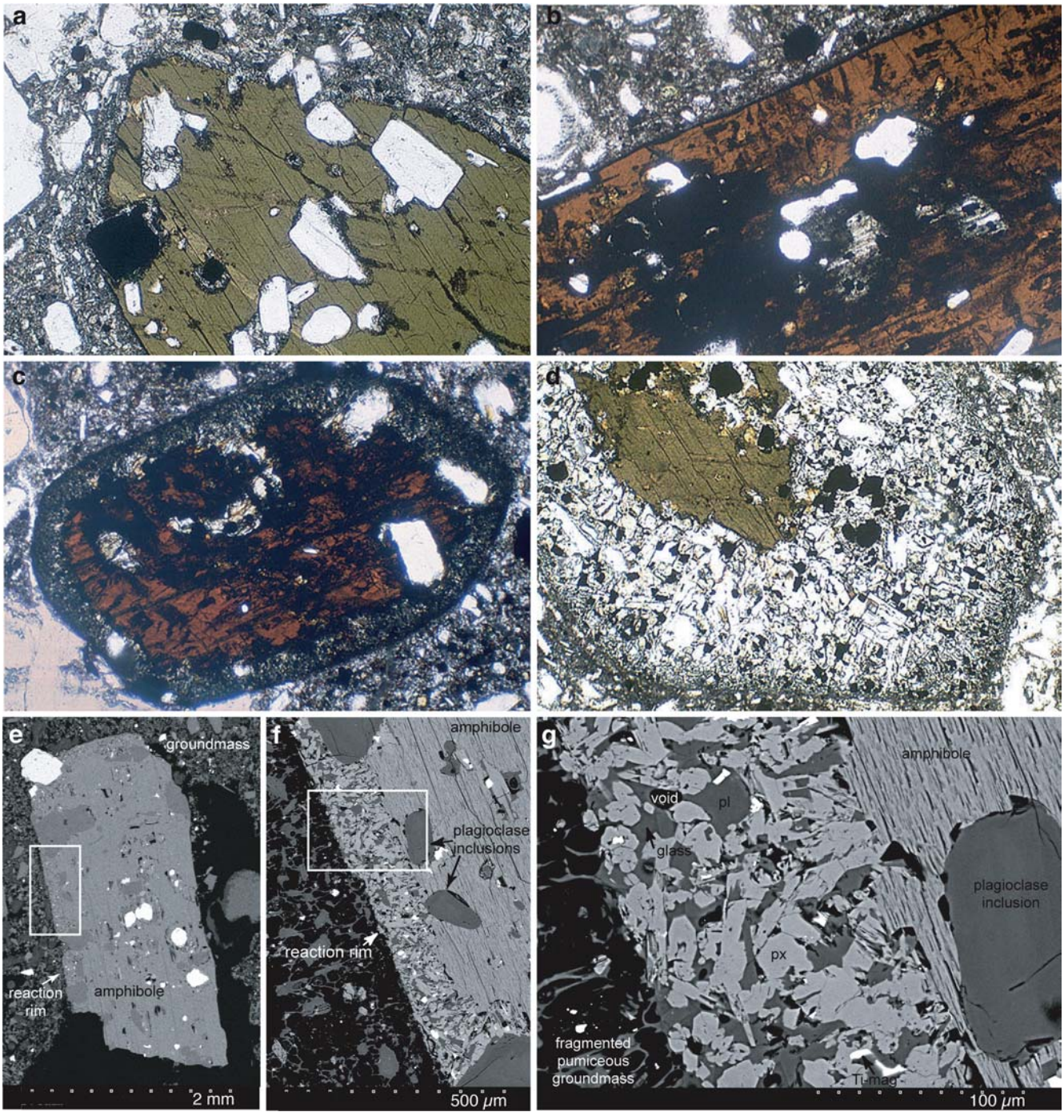

Fig. 1 Photomicrographs of hornblende reaction rims. **a** Large pristine hornblende phenocryst. **b** Hornblende phenocryst with fine-grained reaction rim. The crystal is brown due to oxidation and parts of the crystal display opacitisation (cf Garcia and Jacobson 1979). **c** Large brown hornblende phenocryst displaying extensive areas of opacitisation and decompression-induced reaction rim. **d** Hornblende phenocryst with extensive coarse-grained reaction rim (after Murphy et al. 2000, with permission). The original outline of the crystal is clearly visible. **a**–**d** Photomicrographs from a collection by M. Murphy, of the 1995–1999 eruption products of Soufrière Hills Volcano, Montserrat. All are in transmitted light. Field of view is ~3 mm in all cases. **e**–**g** Backscattered electron (BSE) images of the reacted hornblende phenocryst studies from sample MVO1090B. The reaction rim is only preserved on two sides of the phenocryst. The boxes in (**e**) and (**f**) show the reaction rim areas enlarged in following frames. Minerals, glass and voids are represented by different greyscale levels, reflecting compositional differences. The hornblende reaction rim contains pyroxene (px), plagioclase (pl), titanomagnetite (Ti-mag) and glass

investigated. Coexisting glasses were also characterised in these samples: matrix glass, melt inclusions in amphibole phenocrysts and glass within reaction rims. Unreacted amphibole phenocrysts were analysed in other contemporaneous samples to determine whether any compositional heterogeneity might exist within the

Table 1 List of samples from Soufrière Hills Volcano, Montserrat, used in this study

Sample no.	Eruption date	Locality	Rock type	Description
Unreacted amphiboles				
MVO182	20 January 1997	Pyroclastic fan	PF deposit	Dark grey, moderately vesicular block
MVO665	26 December 1997	PF at bottom of White River, on top of debris avalanche	PF deposit	Dense, banded hornblende-rich lava block
MVO1091A	1 April 1999	Tar River delta	PF deposit	Dark grey, dense, vesicular block from block and ash flow deposit
Reacted amphiboles				
MVO177	13 January 1997	Pyroclastic fan	PF deposit	Pinkish-grey block
MVO1006w	October 1997	Spanish Point area: pumice lobes on S edge of flows		Andesite matrix surrounding small mafic inclusion
MVO1090B	1 March 1999	Tar River delta	PF deposit	Dense pumiceous blocks from block and ash flow deposit
MVO1217	25 February 2001	White River	PF deposit	

Details in this table derive from the Montserrat Volcano Observatory sample list (1 December 2000, revision), except MVO1217 (S. Couch, personal communication)
PF pyroclastic flow

precursor amphiboles. One representative amphibole phenocryst from each sample was chosen for study.

Electron probe microanalysis

Major element compositions of the minerals were obtained by electron probe microanalysis (EPMA) at the University of Bristol. Most amphibole phenocrysts were analysed on a Cameca Camebax electron microprobe with four wavelength dispersive spectrometers, operated through SAMx automation software. Online data reduction used the ϕ–ρ– z model of Pouchou and Pichoir (1985). Amphibole compositions from sample MVO1217 and mineral phases within all of the amphibole reaction textures were analysed on a JEOL JXA-8600 Superprobe equipped with four spectrometers, LINK analytical X-ray analysis system, LEMAS automation and ZAF online data reduction. All mineral phases were analysed with an accelerating potential of 15 kV, a beam current of 15 nA and minimum beam diameter (~1 μm). Minimum counting times were typically ≥20 s on peak and 8 s on background.

Major element compositions of glasses were also obtained by EPMA at the University of Bristol, using the JEOL JXA-8600 electron probe. EMPA of hydrous silicate glasses is complicated by alkali migration during prolonged heating of unstable samples under an electron beam. This effect can result in significant underestimation of Na and overestimation of Si contents (Morgan and London 1996). Harford et al. (2003) have determined optimum conditions for EPMA of Soufrière Hills matrix glasses. Using an accelerating voltage of 15 kV and a 2 nA beam rastered over as large an area as possible (typically ~5×4 μm), with total Na count time limited to 40 s and early analysis of Na, Si and Al, Na-loss can be limited to less than ~5% relative. The same analytical conditions have been adopted in this study. Interstitial glass in reaction rims occupies small areas. Only areas large enough to analyse using the above conditions are reported and many analyses of smaller areas had to be discarded.

Modal analysis

The distribution and proportions of phases throughout hornblende reaction rims were determined by an element mapping approach. This was performed using a Cambridge S250 Mk3 Stereoscan scanning electron microscope (SEM) fitted with a PCXA energy-dispersive X-ray analyser. Relative X-ray intensities were mapped for several diagnostic elements (Si, Ti, Al, Fe, Mg, Ca and K) known to be concentrated preferentially, either individually or in combination, in one or more phases of interest (i.e. K in volcanic glass, Fe and Ti in magnetite, Al in plagioclase, Mg and Fe in pyroxene together with Ca to distinguish clinopyroxene from orthopyroxene). All elements were scanned in energy-dispersive mode with an operating voltage of 20 kV and dwell time of 100 ms. This technique was only performed after EPMA so that quantitative compositional data would not suffer from sodium mobilisation resulting from mapping. Resulting BSE digital images or maps for each element were then scaled to the best resolution attainable (~1 μm per pixel) and analysed using image processing software (NIH image) to quantify areas of high BSE count density. Areal fractions were converted to mass fractions using the following phase densities (g cm^{-3}): plagioclase = 2.7, clinopyroxene = 3.3, orthopyroxene = 3.5 and Fe-oxides = 5.2.

Reaction rim width measurement

Reaction rim widths were measured and scaled from magnified BSE images of the rims, obtained by SEM. Precise measurements of rim widths are possible by this method because the rims preserve the euhedral morphology of the precursor amphibole and display

relatively uniform thickness around a given crystal. Misleading depth effects encountered in transmitted light techniques are avoided as back-scattered electrons sample only the phases exposed near the thin section surface (Rutherford and Hill 1993). Reaction rim widths are displayed most accurately normal to the crystal faces that they replace. These are best displayed and most easily identified in grains cut perpendicular to the *c*-axis (two good cleavages) and on faces (011), and in grains cut normal to the a axis (one good cleavage and straight extinction). Where hornblendes retain a substantial core crystal orientation can be determined optically.

Mineral chemistry

Amphibole

Amphibole phenocrysts are abundant in the recent Soufrière Hills andesite. These have been described in detail by Murphy et al. (2000) and Rutherford and Devine (2003). Most are large (0.5–1.5 cm) and green to brown in colour, with euhedral to anhedral form. Inclusions of plagioclase and titanomagnetite are common, as well as occasional melt inclusions. All are calcic amphiboles; magnesiohornblendes in the terminology of Leake et al. (1997). Rutherford and Devine (2003) have observed compositional zoning in some hornblende phenocrysts, with zones of higher Mg and Si grading gradually outwards to darker-coloured zones depleted in these elements and enriched in Fe and Al. The total compositional variation is small; ≤ 2 wt% change each in SiO_2, MgO, FeO and Al_2O_3. Multiple zones are common and up to seven have been identified in large phenocrysts.

The composition required for material balance calculations is that of reacted hornblende. This must be reconstructed from remnant hornblende material. Suitable proxies for the reacted amphibole are either unreacted phenocryst rims, or the outermost region of remnant cores surviving in reacted phenocrysts. The choice between these depends on whether pristine hornblende phenocrysts have the same chemistry as those with reaction rims, and whether compositional zoning in the reactant hornblende is likely. Compositions of unreacted and reacted SHV hornblendes are given in Table 2. Both core and rim compositions are reported, though for reacted phenocrysts the rim composition is for the outermost remaining hornblende, not the original rim material. No compositional zonation is optically discernable in these hornblendes. This could either be because none is present, or because zoning is less visible in near-basal sections, as used in this study, than in crystals sectioned parallel to the crystallographic *c*-axis (Rutherford and Devine 2003).

Comparing core compositions from Table 2, and allowing for uncertainties of $\pm 2\sigma$ in the mean composition for each sample, no significant difference between unreacted and reacted phenocryst core chemistry is evident. Compositions correspond most closely to those of the MgO and SiO_2 enriched zones reported by Rutherford and Devine (2003); approximately 48–49 wt% SiO_2, 6–7 wt% Al_2O_3, 14–15 wt% FeO^T and 14.5–15 wt% MgO. Only one phenocryst (MVO1217) displays the MgO and SiO_2-depleted composition, as observed by Rutherford and Devine (2003) towards the outer margins of zones (around 46 wt% SiO_2, 8–9 wt% Al_2O_3, 15–16 wt% FeO^T and 13.5–14 wt% MgO). Compositions of both unreacted and reacted rims are consistent with core compositions within error.

Reaction rim assemblage

Fine-grained (~5–70 μm) reaction rims are composed of intergrowths of clinopyroxene, orthopyroxene, plagioclase and Fe–Ti oxide(s) (Fig. 1). Glass is present within the reaction rims as interstitial patches between the mineral grains. This glass is compositionally similar to the surrounding matrix glass, perhaps indicating that glass in reaction rims originated as matrix melt that infiltrated permeable hornblende reaction rims, rather than as a direct product of the hornblende breakdown reaction. Alternatively interstitial reaction rim melt could have equilibrated with the matrix melt by diffusion during rim formation.

Pyroxene

Clinopyroxene and orthopyroxene are the most abundant phases in the hornblende reaction rims, comprising approximately 53 and 23% of the mode, respectively. Both cpx and opx crystals display a variety of morphologies, ranging from small (~10 μm) rounded anhedral grains to larger (~70 μm) elongate dendritic, skeletal or tabular laths. No preferred orientation of the crystals is observed. Pyroxene compositions within the reaction rims are variable; clinopyroxene has $En_{40\text{-}50}$ and $Wo_{27\text{-}41}$ and orthopyroxene has $En_{61\text{-}67}$ and $Wo_{3\text{-}6}$ (Table 3). These compositions fall within the range of groundmass pyroxene, and clinopyroxene microphenocryst compositions in recent Soufrière Hills andesite (Murphy et al. 2000), although clinopyroxene in reaction rims has slightly lower average Wo and En (Fig. 2). No systematic variation is observed between pyroxene composition and depth into the reaction rim (Fig. 3a).

Plagioclase

Plagioclase accounts for approximately 18% of the reaction rim mode. Crystals have subhedral and tabular morphologies, typically being smaller (~5–50 μm) than the surrounding pyroxenes. Plagioclase compositions vary over the range $An_{53\text{-}64}$ (Table 4, Fig. 4), consistent with compositions of sodic rims of calcic microphenocrysts (Murphy et al. 2000) and groundmass microlites in both pumices and dome rocks (Murphy

Table 2 Representative average amphibole compositions

Sample	Unreacted amphiboles								Reacted amphiboles							
	MVO182		MVO665		MVO1091A		MVO177		MVO1006w		MVO1090B		MVO1217			
	Core	Rim	Core	Rim	Core	Rim	Core	Rim	Core	Rim	Core	Rim	Core	Rim		
n	13	14	14	15	12	10	19	15	12	13	12	12	8	8		
SiO_2	47.72 *0.67*	46.76 *0.53*	47.32 *0.49*	48.24 *0.35*	46.67 *0.95*	47 *0.58*	47.49 *0.84*	47.72 *0.45*	48.19 *0.53*	48.15 *0.45*	48.15 *1.22*	48.11 *0.87*	46.99 *0.87*	47.17 *0.4*		
TiO_2	1.46 *0.08*	1.57 *0.07*	1.48 *0.1*	1.58 *0.1*	1.33 *0.08*	1.44 *0.06*	1.38 *0.11*	1.44 *0.11*	1.38 *0.07*	1.43 *0.05*	1.33 *0.1*	1.37 *0.15*	1.63 *0.17*	1.71 *0.16*		
Al_2O_3	6.83 *0.34*	7.48 *0.45*	7.51 *0.36*	6.8 *0.28*	7.47 *0.29*	7.43 *0.28*	6.95 *0.41*	6.62 *0.56*	6.61 *0.39*	6.78 *0.36*	7.55 *0.66*	7.14 *0.26*	7.12 *0.71*	7.09 *0.38*		
FeO^T	14.71 *0.38*	15.41 *0.44*	14.66 *0.34*	13.3 *0.43*	15.37 *0.25*	13.98 *0.49*	14.79 *0.76*	14.42 *0.42*	14.6 *0.36*	14.53 *0.34*	14.33 *0.7*	14.43 *0.46*	15.24 *0.63*	15.31 *0.25*		
MnO	0.54 *0.05*	0.64 *0.23*	0.55 *0.08*	0.4 *0.06*	0.55 *0.05*	0.4 *0.05*	0.55 *0.05*	0.5 *0.06*	0.52 *0.05*	0.52 *0.05*	0.45 *0.08*	0.49 *0.09*	0.55 *0.03*	0.53 *0.06*		
MgO	13.94 *0.36*	13.49 *0.29*	13.79 *0.2*	14.85 *0.33*	14.55 *0.26*	15.21 *0.3*	13.82 *0.59*	14.16 *0.72*	14.17 *0.41*	14.16 *0.3*	13.69 *0.42*	13.83 *0.16*	13.72 *0.58*	13.95 *0.25*		
CaO	11.29 *0.15*	11.15 *0.16*	11.01 *0.14*	11.46 *0.15*	10.73 *0.11*	11.27 *0.08*	11.1 *0.39*	11.13 *0.1*	11.12 *0.12*	11.19 *0.08*	10.72 *0.31*	10.88 *0.22*	11.18 *0.72*	10.99 *0.1*		
Na_2O	1.22 *0.07*	1.35 *0.1*	1.37 *0.08*	1.29 *0.08*	1.33 *0.06*	1.33 *0.06*	1.3 *0.13*	1.27 *0.08*	1.25 *0.1*	1.3 *0.08*	1.39 *0.07*	1.35 *0.06*	1.4 *0.18*	1.43 *0.11*		
K_2O	0.17 *0.03*	0.19 *0.02*	0.17 *0.02*	0.15 *0.02*	0.13 *0.02*	0.13 *0.02*	0.2 *0.07*	0.16 *0.03*	0.18 *0.02*	0.19 *0.02*	0.23 *0.04*	0.21 *0.02*	0.2 *0.04*	0.18 *0.03*		
Total	97.88	98.04	97.85	98.07	98.12	98.2	97.58	97.43	98.01	98.26	97.84	97.81	98.04	98.36		
Si^{4+}	6.923 *0.065*	6.803 *0.064*	6.863 *0.06*	6.946 *0.046*	6.763 *0.071*	6.773 *0.048*	6.917 *0.1*	6.953 *0.059*	6.973 *0.061*	6.953 *0.05*	6.966 *0.106*	6.973 *0.079*	6.852 *0.112*	6.848 *0.052*		
Ti^{4+}	0.16 *0.01*	0.172 *0.008*	0.162 *0.012*	0.171 *0.011*	0.145 *0.009*	0.156 *0.007*	0.152 *0.012*	0.158 *0.012*	0.15 *0.008*	0.155 *0.006*	0.145 *0.011*	0.15 *0.017*	0.179 *0.021*	0.187 *0.018*		
$Al^{(IV)}$	1.077 *0.065*	1.197 *0.064*	1.137 *0.06*	1.054 *0.046*	1.237 *0.071*	1.227 *0.048*	1.083 *0.1*	10.43 *0.073*	1.027 *0.061*	1.047 *0.05*	1.034 *0.106*	1.028 *0.079*	1.148 *0.112*	1.152 *0.052*		
$Al^{(VI)}$	0.092 *0.024*	0.085 *0.03*	0.146 *0.02*	0.1 *0.036*	0.04 *0.021*	0.035 *0.014*	0.109 *0.077*	0.094 *0.036*	0.1 *0.034*	0.106 *0.033*	0.253 *0.102*	0.192 *0.065*	0.08 *0.027*	0.06 *0.036*		
Fe^{3+}	0.547 *0.055*	0.602 *0.075*	0.559 *0.061*	0.47 *0.059*	0.657 *0.044*	0.612 *0.06*	0.55 *0.14*	0.494 *0.108*	0.526 *0.071*	0.513 *0.061*	0.454 *0.108*	0.46 *0.081*	0.546 *0.072*	0.483 *0.063*		
Fe^{2+}	1.238 *0.05*	1.272 *0.069*	1.22 *0.037*	1.131 *0.065*	1.205 *0.059*	1.073 *0.101*	1.252 *0.077*	1.263 *0.068*	1.24 *0.069*	1.242 *0.066*	1.28 *0.055*	1.289 *0.039*	1.328 *0.05*	1.375 *0.075*		
Mn^{2+}	0.066 *0.006*	0.079 *0.027*	0.068 *0.01*	0.049 *0.007*	0.067 *0.006*	0.049 *0.006*	0.068 *0.006*	0.062 *0.007*	0.063 *0.006*	0.064 *0.006*	0.055 *0.01*	0.061 *0.01*	0.068 *0.005*	0.065 *0.008*		
Mg^{2+}	3.016 *0.062*	2.927 *0.056*	2.982 *0.039*	3.188 *0.063*	3.143 *0.04*	3.268 *0.061*	3.001 *0.109*	3.076 *0.159*	3.055 *0.078*	3.049 *0.056*	2.954 *0.101*	2.989 *0.052*	2.964 *0.124*	3.02 *0.055*		
Ca^{2+}	1.754 *0.015*	1.738 *0.025*	1.71 *0.023*	1.768 *0.022*	1.666 *0.03*	1.74 *0.019*	1.732 *0.061*	1.737 *0.014*	1.724 *0.018*	1.731 *0.015*	1.662 *0.061*	1.69 *0.043*	1.704 *0.014*	1.709 *0.017*		
$Na^{(M4)}$	0.13 *0.009*	0.125 *0.021*	0.146 *0.019*	0.122 *0.017*	0.074 *0.039*	0.067 *0.028*	0.134 *0.039*	0.129 *0.037*	0.138 *0.022*	0.14 *0.012*	0.198 *0.043*	0.171 *0.036*	0.131 *0.022*	0.102 *0.043*		
$Na^{(A)}$	0.216 *0.02*	0.255 *0.033*	0.238 *0.031*	0.245 *0.043*	0.299 *0.051*	0.306 *0.039*	0.234 *0.039*	0.23 *0.026*	0.212 *0.031*	0.223 *0.025*	0.197 *0.047*	0.208 *0.042*	0.26 *0.033*	0.303 *0.044*		
K^+	0.032 *0.005*	0.035 *0.004*	0.032 *0.005*	0.027 *0.004*	0.023 *0.004*	0.023 *0.005*	0.037 *0.013*	0.03 *0.005*	0.034 *0.004*	0.036 *0.005*	0.043 *0.007*	0.064 *0.087*	0.036 *0.007*	0.033 *0.005*		
Total	15.249	15.291	15.262	15.271	15.322	15.328	15.268	15.268	15.242	15.258	15.24	15.272	15.296	15.336		

Each column is the average composition of the core or rim of a single phenocryst (*n* number of analyses). Core and rim analyses for a given sample refer to the same crystal. In the case of reacted hornblendes, the original rim no longer exists, so rim compositions refer to the outer edge of remnant cores. Figures in italics indicate one standard deviation on the reported average compositions. The structural formula was calculated for every analysis in order to determine the standard deviation on cation proportions. Cation proportions are calculated on the basis of 23 oxygens using the average ferric method of Leake et al. (1997)

Table 3 Representative average compositions of pyroxenes in hornblende reaction rims

Sample	Orthopyroxene				Clinopyroxene			
	MVO177	MVO1006w	MVO1090B	MVO1217	MVO177	MVO1006w	MVO1090B	MVO1217
No. of analyses	10	11	12	15	17	5	10	11
SiO_2	52.54	52.59	52.5	52.29	51.05	50.98	51.04	50.22
TiO_2	0.33	0.3	0.38	0.6	0.67	0.63	0.83	1.04
Al_2O_3	1.72	1.57	1.77	2	2.36	2.31	2.58	2.89
FeO^T	19.5	19.63	20.2	18.62	12.04	12.13	12.75	13.01
MnO	0.87	0.8	0.88	0.74	0.64	0.62	0.67	0.61
MgO	23.09	22.72	22.16	23.59	15.29	15.04	14.7	15.85
CaO	1.76	1.8	1.92	2.15	17.75	17.59	17.01	16.09
Na_2O	0.03	0.04	0.05	0.08	0.21	0.19	0.25	0.2
K_2O	0.04	0.01	0.01	0.02	0.02	0.01	0.02	0.01
Total	99.88	99.47	99.86	100.09	100.03	99.5	99.85	99.93
Si^{4+}	1.946	1.956	1.951	1.928	1.915	1.922	1.92	1.888
Ti^{4+}	0.009	0.009	0.011	0.017	0.019	0.018	0.024	0.03
Al^{3+}	0.075	0.069	0.077	0.087	0.105	0.103	0.115	0.128
Fe^{2+}	0.604	0.611	0.628	0.574	0.378	0.383	0.401	0.409
Mn^{2+}	0.027	0.026	0.028	0.023	0.02	0.02	0.022	0.019
Mg^{2+}	1.275	1.26	1.227	1.297	0.855	0.846	0.824	0.888
Ca^{2+}	0.07	0.072	0.076	0.085	0.714	0.713	0.686	0.649
Na^{+}	0.002	0.003	0.004	0.006	0.015	0.014	0.018	0.015
Total	4.008	4.005	4.001	4.015	4.02	4.018	4.008	4.026
Oxygen	6	6	6	6	6	6	6	6
En	0.645	0.64	0.627	0.655	0.435	0.431	0.426	0.452
Fs	0.319	0.323	0.335	0.29	0.202	0.205	0.219	0.208
Wo	0.035	0.037	0.039	0.043	0.363	0.363	0.355	0.33
En (max)	0.66	0.655	0.654	0.668	0.502	0.444	0.467	0.494
En (min)	0.627	0.624	0.608	0.635	0.399	0.422	0.398	0.407
Fs (max)	0.331	0.346	0.359	0.331	0.236	0.217	0.238	0.236
Fs (min)	0.306	0.304	0.307	0.306	0.176	0.198	0.193	0.176
Wo (max)	0.048	0.046	0.046	0.062	0.409	0.379	0.402	0.387
Wo (min)	0.029	0.03	0.034	0.035	0.277	0.338	0.307	0.274

Each column is the average composition of either orthopyroxene (opx) or clinopyroxene (cpx) in a single hornblende reaction rim. For each sample opx and cpx compositions have been analysed in the same reaction rim. The average composition given in each column is combined data from several microscopic pyroxene grains within a given reaction rim. Cation proportions are calculated on the basis of six oxygens. Average, minimum and maximum values of the main pyroxene components are given below the analyses

et al. 2000; Couch et al. 2003). No systematic variation is observed between plagioclase composition and depth within the reaction rims (Fig. 3b), although a weak increase in Ab deeper in the rim is indicated within MVO177.

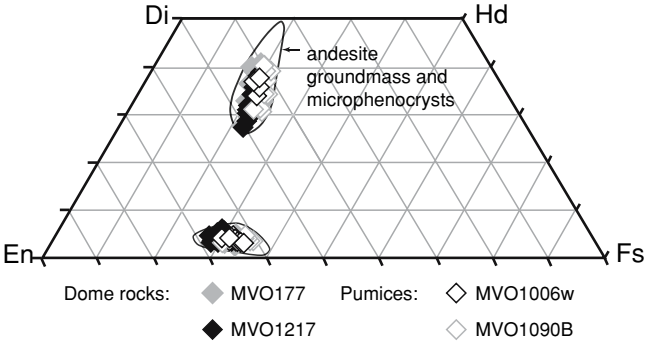

Fig. 2 Pyroxene compositions in hornblende reaction rims, plotted as mol% of the simple quadrilateral components. Compositions of the main SHV groundmass pyroxene populations (including clinopyroxene microphenocrysts) determined by Murphy et al. (2000) are also shown (*outlined fields*) for comparison

Fe-oxides

In three of the reaction rims studied (MVO177, MVO1006w and MVO1090B) titanomagnetite is the only oxide phase present, accounting for about 5% of the mode. Crystals are typically small (~5–30 μm) anhedral grains. Compositions are variable, typically spanning the range $Usp_{10\text{-}26}$; the overall range extending to Usp_{54}. Almost as much chemical variation is present within a single reaction rim as between the three rims studied, and no spatial relationship is observed (Fig. 3c). Magnetite and ilmenite rather than titanomagnetite were found in the remaining reaction rim (sample MVO1217), each comprising approximately 2% of the mode. For both minerals crystals are small (~5–30 μm) and anhedral. Compositions are shown in Table 5 and Fig. 5.

Material balance calculations and estimates of material transport

Mass balance calculations were performed between the reactant hornblende and the product reaction rim

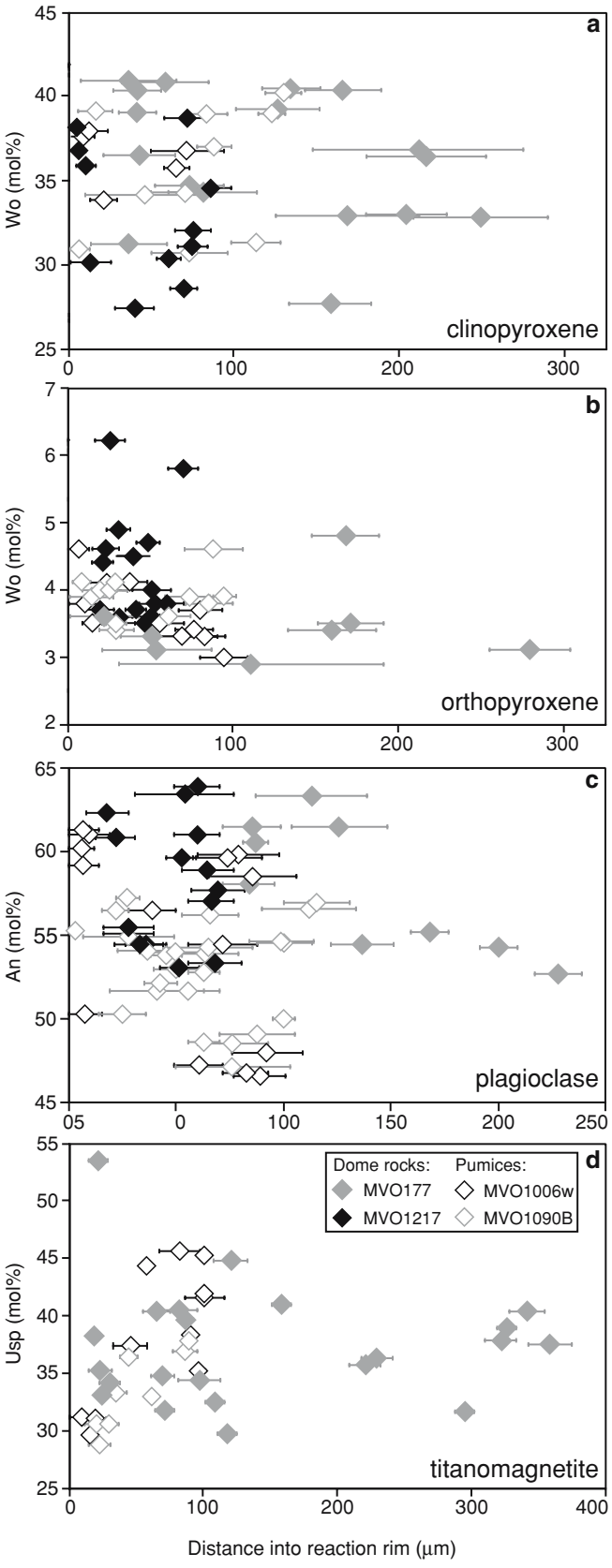

Fig. 3 Plot illustrating the variation in product mineral compositions across the width of reaction rims. Distances on the *x*-axis increase towards the inner reaction rim boundary with hornblende. Each *plot symbol* refers to a single reaction rim. Each *data point* represents the composition and position of a single crystal within the reaction rim. *Error bars* indicate the maximum dimension of each crystal normal to the reaction rim margins. **a** Pyroxene compositions are expressed in mol% Wo. **b** Plagioclase compositions are expressed in mol% An. A weak decrease in An with depth into the rim is indicated within MVO177, for which the line of best fit (*not shown*) is linear with a correlation coefficient (R^2) of 0.6. **c** Titanomagnetite compositions expressed in mol% Usp

Table 4 Representative average compositions of plagioclase in hornblende reaction rims

Sample	MVO177	MVO1006w	MVO1090B	MVO1217
No. of analyses	9	13	23	15
SiO_2	53.83	54.14	54.35	52.99
TiO_2	0.03	0.04	n.d.	0.23
Al_2O_3	29.03	28.35	28.11	29.04
FeO^T	0.87	0.83	0.55	1.04
MnO	0.05	0.05	n.d.	0.02
MgO	0.06	0.14	0.03	0.1
CaO	11.9	11.66	11.15	12.1
Na_2O	4.69	5.06	5.1	4.75
K_2O	0.12	0.14	0.13	0.13
Total	100.58	100.41	99.42	100.4
Si^{4+}	2.428	2.446	2.467	2.404
Ti^{4+}	0.001	0.001		0.008
Al^{3+}	1.544	1.512	1.504	1.553
Fe^{2+}	0.033	0.031	0.021	0.039
Mn^{2+}	0.002	0.004		0.001
Mg^{2+}	0.004	0.009	0.002	0.007
Ca^{2+}	0.575	0.565	0.542	0.588
Na^{+}	0.410	0.444	0.449	0.418
K^{+}	0.007	0.008	0.008	0.008
Total	5.007	5.021	5.004	5.025
Oxygen	8	8	8	8
An	0.580	0.556	0.543	0.580
Ab	0.413	0.436	0.449	0.412
Or	0.005	0.008	0.008	0.008
An (max)	0.633	0.624	0.572	0.639
An (min)	0.527	0.466	0.471	0.531

Each column is the average composition of plagioclase in a single hornblende reaction rim. The average composition given in each column is combined data from several microscopic plagioclase grains within a given reaction rim. Cation proportions are calculated on the basis of eight oxygens. Average values of the main feldspar components are given as well as minimum and maximum An contents measured within each reaction rim*n.d.* not detected

phases, using the linear least squares petrologic mixing program 'Petmix' of Wright and Doherty (1970). The program was used according to the method for calculation of a chemical mode. Given the bulk chemical composition of a rock, in terms of element oxides, together with the chemical compositions of its constituent minerals, the program will calculate the modal mineral proportions (in weight percent) that best fit the rock

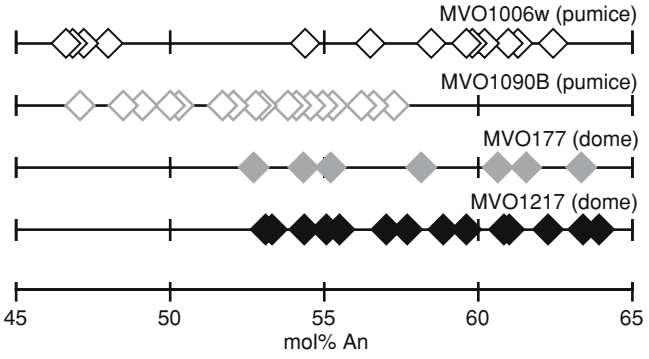

Fig. 4 Plagioclase compositions in hornblende reaction rims, plot as mol% An

Table 5 Representative average compositions of Fe–Ti oxides in amphibole reaction rims

Sample	MVO177	MVO1006w	MVO1090B	MVO1217	MVO1217
No. of analyses	22	11	9	6	6
SiO_2	0.12	0.65	0.28	0.08	0.09
TiO_2	13.12	13.3	11.48	3.74	38
Al_2O_3	2.06	2.61	1.96	1.42	0.13
FeO^T	77.24	73.58	76.31	85.19	54.2
MnO	0.53	0.62	0.64	0.58	1.01
MgO	1.07	1.52	1.69	1.15	2.48
CaO	0.22	0.29	0.28	0.24	0.21
Na_2O	0.04	0.01	0.02	0.01	n.d.
K_2O	0.01	0.02	0.01	0.01	0.01
Total	94.41	92.6	92.67	92.42	96.13
Si^{4+}	0.005	0.024	0.011	0.003	0.003
Ti^{4+}	0.373	0.383	0.33	0.108	1.086
Al^{3+}	0.091	0.118	0.088	0.064	0.006
Fe^{3+}	1.156	1.069	1.232	1.347	
Fe^{2+}	1.285	1.285	1.208	1.384	1.724
Mn^{2+}	0.017	0.02	0.021	0.019	0.032
Mg^{2+}	0.06	0.086	0.096	0.066	0.14
Ca^{2+}	0.009	0.012	0.011	0.01	0.008
Total	3	3	3	3	3
Oxygen	4	4	4		4
Usp	37.3	38.3	33	10.8	
Usp (max)	53.5	45.6	37.9	12.8	
Usp (min)	31.6	29.6	28.8	9.6	

Each column is the average composition of an Fe–Ti oxide phase in a single hornblende reaction rim. Rims in samples MVO177, MVO1006w and MVO1090B contain only titanomagnetite; MVO1217 contains magnetite and ilmenite. The average composition given in each column is combined data from several microscopic oxide grains. Cation proportions are calculated on the basis of four oxygens. Fe^{2+} and Fe^{3+} recalculation used the method of Droop (1987). Average molar proportions of ulvöspinel (Usp) are given along with minimum and maximum Usp contents measured within each reaction rim are also shown, where relevant
n.d. not detected

composition. For the case of the hornblende breakdown reaction, the reactant hornblende is taken as the bulk composition.

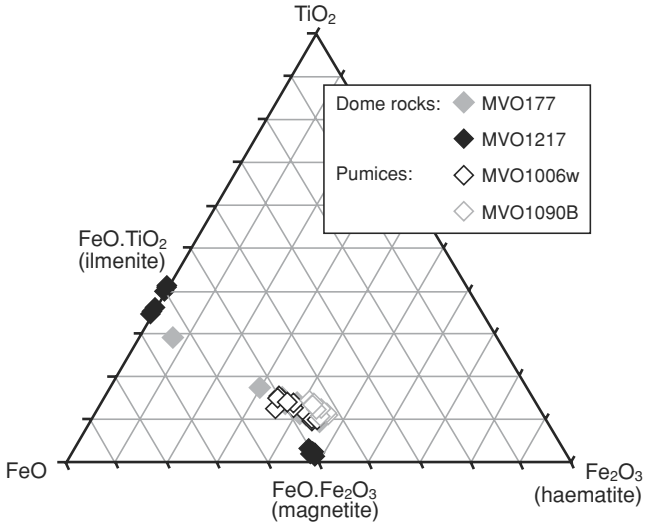

Fig. 5 Fe–Ti oxide compositions in hornblende reaction rims, plot in the system $FeO–Fe_2O_3–TiO_2$ as mol%

Soufrière Hills Volcano

Two slightly different product assemblages have been observed in SHV hornblende reaction rims so we have considered a separate reaction for each:

$$\text{hbl} \rightarrow \text{cpx} + \text{opx} + \text{plag} + \text{Ti - mag} \quad (2)$$

$$\text{hbl} \rightarrow \text{cpx} + \text{opx} + \text{plag} + \text{ilm} + \text{mag} \quad (3)$$

Melt has not been included as a phase in these reactions because neither hornblende alone, nor any single combination of hornblende and melt can exactly reproduce the composition of the reaction rim products. By expressing the reaction as a simple conversion of hornblende to pyroxenes + plagioclase + Fe-oxide(s), the compositional differences between hornblende and the best-fit combination of product phases are clear. It is assumed that these differences are balanced by exchanges with the host melt phase.

The modelling treats minerals as homogeneous phases, so some generalisations about mineral compositions have been made. For the reactant hornblende we have used outermost remnant core compositions as a proxy. This composition (Table 6) is the combined average of all 'rim' data from the four reacted phenocrysts studied. The hornblende volatile content has not been analysed here so compositions have been recast to 100 wt% anhydrous. In the absence of any systematic variation in orthopyroxene, clinopyroxene, plagioclase or titanomagnetite composition between or within reaction rims, compositions of each of these phases have been averaged over the three samples displaying reaction 2 and normalised to 100 wt% (Table 6). Compositions of mineral phases in the reaction rim from MVO1217 have been treated separately, and input mineral compositions for

Table 6 Input parameters and results of Soufrière Hills Volcano hornblende breakdown material balance calculations using the PETMIX petrologic mixing program

	Input parameters												Output		Uncertainties[b]		
	Hornblende		Orthopyroxene		Clinopyroxene		Plagioclase		Magnetite	Titanomagnetite		Ilmenite	Bulk rim	Residuals[a]	Reactant	Products	Residuals[c]
Reaction 2: Hbl → Cpx + Opx + Plag + Ti-mag (samples MVO177, MVO1006w and MVO1090B)													100.0 Hbl → 49.8 Cpx + 27.6 Opx + 18.2 Plag + 4.5 Ti-mag				
n	48		33		32		45			42							
SiO_2	48.87	0.68	52.68	0.50	51.09	0.96	54.43	1.27		0.32	0.63		49.87	−1.00	0.20	0.19	−0.86
TiO_2	1.50	0.17	0.34	0.06	0.71	0.23	0.05	0.08		14.22	3.23		1.09	0.41	0.05	0.06	0.37
Al_2O_3	7.02	0.47	1.69	0.43	2.43	0.85	27.86	1.17		2.32	0.58		6.84	0.18	0.14	0.17	0.07
FeO^T	14.91	0.50	19.85	0.73	12.29	0.92	0.91	0.23		80.72	2.39		15.36	−0.45	0.14	0.18	−0.33
s16MnO	0.52	0.07	0.85	0.09	0.65	0.11	0.05	0.07		0.68	0.07		0.60	−0.08	0.02	0.02	−0.07
MgO	14.34	0.47	22.69	0.67	15.08	1.04	0.16	0.19		1.42	0.46		13.86	0.48	0.14	0.19	0.36
16CaO	11.30	0.18	1.84	0.23	17.52	1.64	11.33	0.96		0.27	0.17		11.30	0.00	0.05	0.29	0.15
Na_2O	1.35	0.10	0.04	0.04	0.22	0.06	5.08	0.52		0.03	0.04		1.04	0.31	0.03	0.03	0.29
K_2O	0.19	0.03	0.02	0.04	0.02	0.02	0.13	0.07		0.02	0.01		0.04	0.15	0.01	0.01	0.14
Total	100.00		100.00		100.00		100.00			100.00			100.00				
Reaction 3: Hbl → Opx + Cpx + Plag + Mag + Ilm (sample MVO1217)													100.0 Hbl → 53.9 Cpx + 24.4 Opx + 18.1 Plag + 1.9 Ilm + 1.7 Mag				
n	48		15		11		15			6			6				
SiO_2	48.87	0.68	52.24	0.67	50.26	0.82	52.78	0.91		0.08	0.02		0.09	0.04	49.39	−0.52	0.20	0.29	−0.34
TiO_2	1.50	0.17	0.60	0.19	1.05	0.24	0.23	0.11		4.04	0.49		39.53	2.75	1.58	−0.08	0.05	0.09	−0.03
Al_2O_3	7.02	0.47	1.99	0.67	2.89	0.64	28.92	0.59		1.54	1.02		0.14	0.06	7.30	−0.28	0.14	0.23	−0.15
FeO^T	14.19	0.50	18.60	0.65	13.02	0.79	1.03	0.08		92.19	1.37		56.38	2.53	14.39	−0.20	0.14	0.27	−0.05
s16MnO	0.52	0.07	0.74	0.06	0.61	0.09	0.02	0.02		0.63	0.06		1.05	0.22	0.54	−0.02	0.02	0.03	0.00
MgO	14.34	0.47	23.57	0.95	15.86	1.15	0.10	0.04		1.24	0.16		2.58	0.46	14.39	−0.05	0.14	0.39	0.00
16CaO	11.30	0.18	2.15	0.36	16.10	1.76	12.05	0.79		0.25	0.06		0.22	0.08	11.39	−0.09	0.05	0.58	0.00
Na_2O	1.35	0.10	0.08	0.19	0.20	0.04	4.73	0.40		0.01	0.01		0.00	0.01	0.98	0.37	0.03	0.05	0.34
K_2O	0.19	0.03	0.02	0.04	0.01	0.01	0.13	0.04		0.01	0.01		0.01	0.01	0.03	0.16	0.01	0.01	0.15
Total	100.00		100.00		100.00		100.00			100.00			100.00		100.00				

The reactant hornblende composition is the average of outermost remnant core compositions for reacted hornblende phenocrysts

Reaction 2: Orthopyroxene, clinopyroxene, plagioclase and titanomagnetite compositions are each averages of combined data for the given phase in reaction rims from samples MVO177, MVO1006w and MVO1090B

Reaction 3: Orthopyroxene, clinopyroxene, plagioclase, magnetite and ilmenite compositions are averages for sample MVO1217

Where present, volatiles have been ignored, and in all cases solids have been normalised to 100 wt%. Figures in italics indicate one standard deviation of the reported average compositions. *n* number of analyses

Bulk rim compositions are bulk reaction rim compositions output by the PETMIX program (Wright and Doherty 1970) corresponding to the best-fit combinations of the input reactant compositions. Best-fit reactions are given for each product assemblage above the respective results

[a]The difference between the measured reactant hornblende composition and the calculated bulk reaction rim composition. Positive residuals indicate that the reactant hornblende is enriched relative to the bulk reaction rim and that residual material is released by the reaction. The converse is true for negative residuals

[b]Uncertainties in the reactant and product compositions are two standard errors

[c]Residuals remaining beyond propagated uncertainties in reactant and product compositions

reaction 3 products are normalised averages over the individual reaction rim (Table 6).

Results of the material balance calculations are given in the output section of Table 6. The best-fit solutions indicate the following mass balances for the two reactions:

$$100.0\,\text{hbl} \rightarrow 49.8\,\text{cpx} + 27.6\,\text{opx} + 18.2\,\text{plag} + 4.5\,\text{Ti - mag} \quad (2a)$$

$$100.0\,\text{hbl} \rightarrow 53.9\,\text{cpx} + 24.4\,\text{opx} + 18.1\,\text{plag} + 1.9\,\text{ilm} + 1.7\,\text{mag} \quad (3a)$$

These results agree well with modal analysis of the reaction rim assemblage converted to mass fractions. However, the crystalline phases in the reaction rims do not exactly reproduce the reactant hornblende composition when combined in the proportions indicated by reactions 2a and 3a (bulk rim compositions, Table 6). The amounts by which the reactant and bulk products differ (residuals) are relatively small (≤ 1.00 wt% in magnitude in all cases), and vary in magnitude and sense for each element, and between the two reactions. Positive residuals indicate that reactant hornblende is enriched in a given element relative to the bulk reaction rim, and that the residual material is released by the reaction. Negative residuals indicate that the reaction cannot have occurred without addition of material from the chemical system beyond the hornblende phenocryst. However, residuals given by Petmix need to be compared with uncertainties in input compositions to establish whether the apparent differences can be regarded as significant or within uncertainties.

We calculated uncertainties of two standard errors for the reactant and combined product compositions (uncertainties, Table 6) to minimise residuals from Petmix. For most elements, residuals remain beyond these uncertainties (all elements in reaction 2a; SiO_2, TiO_2, Al_2O_3, FeO^T, Na_2O and K_2O in reaction 3a). These results are consistent with reaction between hornblende phenocrysts and the surrounding melt in an open chemical system, with exchange of most elements. The reaction is inferred to consume SiO_2 and sometimes FeO^T from the melt, and release Na_2O, K_2O and perhaps TiO_2 and MgO into the melt. Volatiles (H_2O and Cl) must also be released by the reaction. If any compositional zoning were present in the reactant hornblende, the likely trend would have been towards lower MgO and SiO_2 and higher FeO^T and Al_2O_3 based on the observations of Rutherford and Devine (2003). This would help to reduce shortfalls in FeO^T but increase shortfalls in SiO_2. Finally we note that variations in magnetite composition and in oxide phase proportions (between reactions 2a and 3a) may reflect variations in fO_2 during the reactions. Such variation in fO_2 might relate to detailed differences in degassing histories, since water exsolution can cause strong oxidation (Candela 1986).

MSH 1980–1986 eruptions

We have made material balance calculations for the compositional data of Rutherford and Hill (1993), using the same approach as for SHV above. We tested each of the five amphibole compositions reported by Rutherford and Hill (1993) as the reactant, against the MSH product rim phase compositions of Rutherford and Hill (1993) in material balance calculations using Petmix as before. The smallest residuals were achieved using the SH-084 amphibole rim composition as the reactant (Table 7):

$$100.0\,\text{hbl} \rightarrow 43.0\,\text{cpx} + 24.5\,\text{opx} + 23.7\,\text{plag} + 5.2\,\text{mag} + 3.5\,\text{ilm} \quad (4)$$

This reaction is markedly different to that proposed by Rutherford and Hill (1993):

$$73\,\text{amph} + 27\,\text{melt} \rightarrow 29\,\text{opx} + 24\,\text{cpx} + 43\,\text{plag} + 3\,\text{ilm} \quad (5)$$

The new calculations here are based on MSH hornblende rim compositions rather than a composition averaged over an entire crystal as in the calculations of Rutherford and Hill (1993). Hornblende phenocrysts in MSH dacites show considerable compositional variation and are commonly zoned: rims are commonly enriched in FeO and SiO_2, and depleted in Al_2O_3 and MgO relative to the cores (Rutherford and Hill 1993). Melt has not been included either as a product or reactant phase in this study. It is assumed instead that exchanges with the melt phase account for any residuals. Thus not all components in the melt have to contribute to the reaction and that the composition of the melt does not need to remain fixed. Magnetite is included in the product assemblage.

Large residuals (≤ 3.30 wt% in magnitude) are associated with reaction 4, including shortfalls in SiO_2, Fe_2O_3, FeO and TiO_2, and excesses in Al_2O_3, MgO, CaO and Na_2O. Fe_2O_3 has been considered in mass balance calculations for MSH because input reactant and product compositions from Rutherford and Hill (1993) were already adjusted for ferric iron content. Rutherford and Hill (1993) do not report uncertainties for product phase compositions so we were unable to compare these residuals with standard errors. Available uncertainties of two standard errors for the reactant hornblende composition alone are insufficient to account completely for any of the residuals (uncertainties, Table 7). Thus these results are consistent with reaction between hornblende phenocrysts and the surrounding melt in an open chemical system. Based on these results the reaction consumes SiO_2, TiO_2, Fe_2O_3 and FeO from the melt and releases Al_2O_3, MgO, CaO and Na_2O from the hornblende into the melt.

Table 7 Input parameters and results of new Mount St. Helens hornblende breakdown material balance calculations using the PETMIX petrologic mixing program

	Input parameters						Output		Uncertainties[b]		
	Horn-blende	Orthopyroxene	Clinopyroxene	Plagioclase	Magnetite	Ilmenite	Bulk rim	Residuals[a]	Reactant	Products	Residuals[a]
Hbl →	Cpx +	Opx +	Plag +	Mag +	Ilm		100.00 Hbl → 43.0 Cpx + 24.5 Opx + 23.7 Plag + 5.2 Mag + 3.5 Ilm				
n	11	20	4	13	9	11					
SiO_2	44.55 *0.81*	52.41	50.60	57.75	0.00	0.00	48.34	−3.79	0.49	?	−3.30
TiO_2	2.21 *0.20*	0.32	0.55	0.00	12.29	44.00	2.50	−0.29	0.12	?	−0.17
Al_2O_3	10.51 *0.86*	1.08	2.31	26.64	1.61	0.48	7.68	2.83	0.52	?	2.31
Fe_2O_3	2.68 *0.30*	0.68	2.44	0.64	44.04	18.01	4.29	−1.61	0.18	?	−1.43
FeO	12.03 *0.41*	21.18	9.51	0.00	40.21	34.32	12.58	−0.55	0.25	?	−0.30
s16MnO	0.20 *0.04*	0.65	0.47	0.00	0.44	0.58	0.40	−0.20	0.02	?	−0.18
MgO	14.23 *0.39*	21.91	14.11	0.00	1.39	2.61	11.61	2.62	0.24	?	2.38
16CaO	11.28 *0.13*	1.70	19.59	8.21	0.00	0.00	10.80	0.48	0.08	?	0.40
Na_2O	1.98 *0.12*	0.04	0.40	6.50	0.00	0.00	1.72	0.26	0.07	?	0.19
K_2O	0.33 *0.95*	0.03	0.01	0.13	0.00	0.00	0.08	0.25	0.57	?	0.00
Total	100.00	100.00	100.00	100.00	100.00	100.00	100.00				

The reactant hornblende composition is the hornblende rim composition SH-084 of Rutherford and Hill (1993)
Orthopyroxene, clinopyroxene, plagioclase, magnetite and ilmenite compositions are hornblende rim phase compositions of Rutherford and Hill (1993)
Where present, volatiles have been ignored, and in all cases solids have been normalised to 100 wt%. Figures in italics indicate one standard deviation of the reported average compositions. *n* number of analyses
The bulk rim composition is the bulk reaction rim compositions output by the PETMIX program (Wright and Doherty 1970) corresponding to the best-fit combination of the input reactant compositions. The best-fit reaction is given above the results
[a]The difference between the measured reactant hornblende composition and the calculated bulk reaction rim composition. Positive residuals indicate that the reactant hornblende is enriched relative to the bulk reaction rim and that residual material is released by the reaction. The converse is true for negative residuals
[b]Uncertainties in the reactant compositions are two standard errors. Rutherford and Hill (1993) do not report uncertainties for reaction rim phase compositions
[c]Residuals remaining beyond uncertainties of two standard errors in the reactant composition

Melt chemistry

Melt inclusions in hornblende

Scarce melt inclusions in SHV hornblende phenocrysts are small (typically $\sim < 10$ μm diameter) and irregularly shaped. Most samples proved unsuitable for reliable EPMA and compositional data reported here are limited. Melt inclusion compositions range from 69.4 to 71.6 wt% SiO_2 (normalised to 100 wt% anhydrous) in a pumice sample and 71.0–74.8 wt% SiO_2 in a dome sample (Table 8). These compositions lie on a trend similar to other natural SHV glasses (Fig. 6) and are the

Table 8 Melt inclusion compositions in hornblende

Sample number	Composition (wt%)									Unnorm total	Qz′	Or′	Ab′
	SiO_2	TiO_2	Al_2O_3	$FeO^{(T)}$	MnO	MgO	CaO	Na_2O	K_2O				
MVO1090B (pumice)	69.43	0.38	15.73	3.20	0.27	0.62	3.64	4.01	2.73	91.74	22.7	8.2	69.0
	70.55	0.44	15.72	2.57	0.17	0.42	3.09	4.88	2.16	96.23	22.3	7.1	70.6
	71.07	0.63	15.26	2.47	b.d.	0.67	2.70	5.08	2.13	94.97	23.3	8.0	68.6
	71.64	0.32	16.15	1.78	0.11	0.15	2.77	4.95	2.12	94.09	23.8	7.6	68.6
	70.68	**0.44**	**15.71**	**2.50**	**0.14**	**0.46**	**3.04**	**4.74**	**2.28**	**94.26**	**23.0**	**7.7**	**69.2**
	0.94	0.13	0.36	0.58	0.11	0.24	0.43	0.49	0.30				
MVO177 (dome lava)	70.96	0.55	15.53	1.29	0.24	0.22	2.82	4.53	3.84	97.47	23.0	14.7	62.2
	71.15	0.42	16.08	0.85	0.07	0.16	3.43	4.39	3.45	95.72	23.0	11.0	66.0
	72.83	0.31	14.26	1.72	0.04	0.24	2.47	4.00	4.13	96.91	27.5	19.0	53.5
	74.77	0.40	13.35	1.39	0.02	0.18	1.84	3.36	4.70	96.94	31.8	23.5	44.7
	72.43	**0.42**	**14.80**	**1.31**	**0.09**	**0.20**	**2.64**	**4.07**	**4.03**	**96.76**	**26.3**	**17.1**	**56.6**
	1.77	0.10	1.23	0.36	0.10	0.04	0.66	0.52	0.53				

All compositions are normalised to 100% anhydrous for comparison. Totals are unnormalised. Each composition is a single analysis. Compositions in bold type are averages of the reported data for each sample; figures in italics indicate one standard deviation of the average compositions *b.d.* below detection

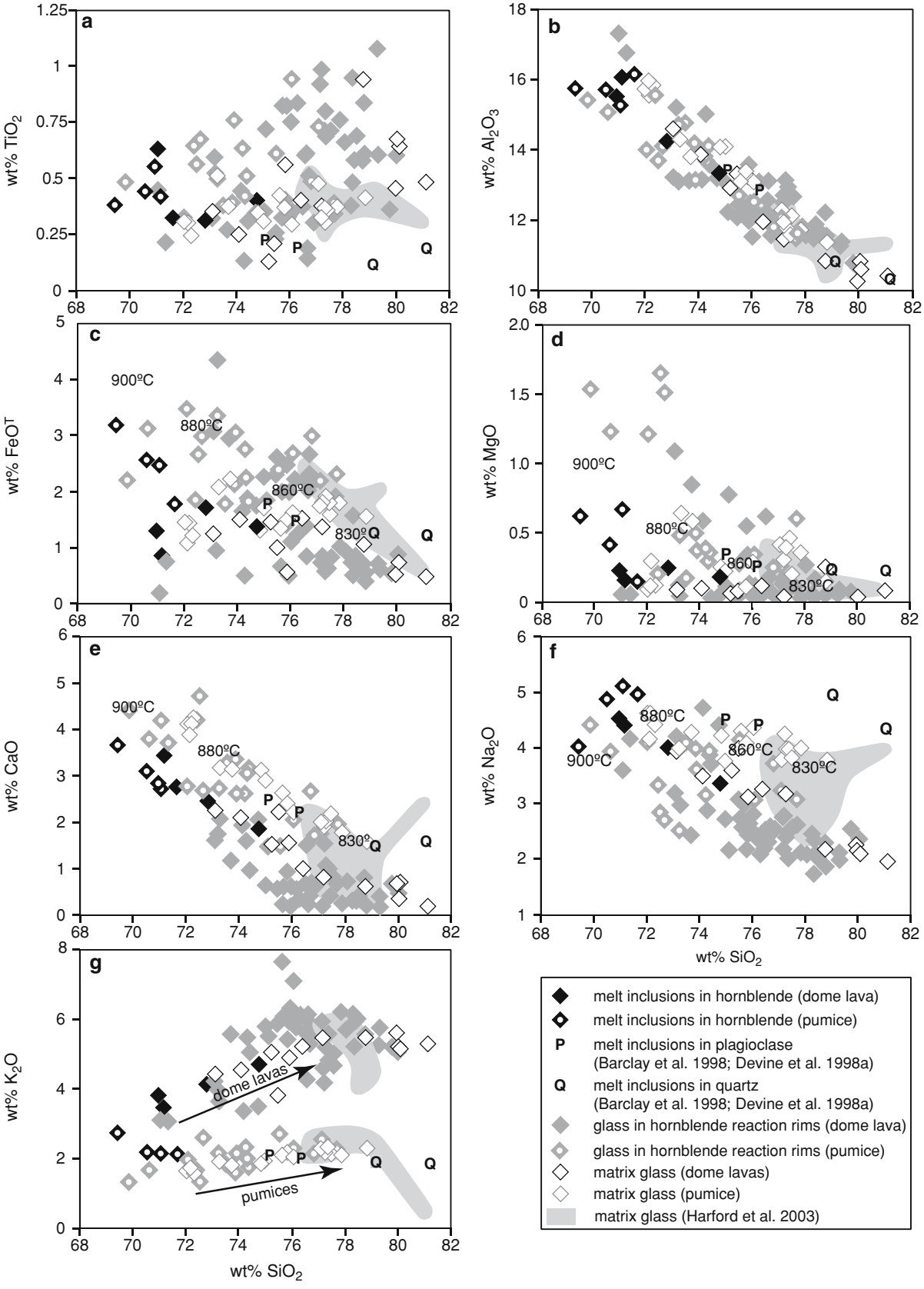

Fig. 6 Harker diagram for Soufrière Hills Volcano glass compositions. Analyses are given in Tables 7, 8 and 9. Temperatures are from Rutherford and Devine (2003)

least evolved melts found so far in SHV andesite. Hornblende melt inclusion compositions are similar to estimates of the groundmass compositions (matrix glass plus crystals smaller than 100 μm; Murphy et al. 2000). This is consistent with hornblende phenocryst growth fairly early in the crystallisation sequence, before significant groundmass crystallisation occurred. Comparison with experimental glass compositions of Rutherford and Devine (2003) indicates temperatures of 900–880°C at water pressures close to 130 MPa for formation of these melt inclusions (Fig. 6). These temperatures are consistent with the maximum estimates of hornblende crystallisation temperatures, based on plagioclase–amphibole thermometry between hornblende phenocrysts and plagioclase inclusions (Couch et al. 2003). Volatile contents estimated using the 'difference method' (100 wt% minus analytical totals equals volatile content; Devine et al. 1995) range from 8.3 to 5.0 wt% in the pumice sample, and 4.3–3.1 wt% in the dome sample. The lower values in melt inclusions in the dome sample may reflect leakage through cracks or along cleavage planes during prolonged magma decompression and residence time in the dome before collapse.

Matrix glasses

Matrix glass is rhyolitic with wide compositional variations (Fig. 6). SiO_2 can vary between 72.0 and 81.1 wt% (normalised to 100 wt% anhydrous; Table 9). Two distinctive groups are present based on sample type; pumice glasses are notably low in K_2O, high in Na_2O and high in CaO, whereas dome glasses are relatively high in K_2O, low in Na_2O and low in CaO. Similar groupings have been recognised in previous studies (Harford et al. 2003; Couch et al. 2003). K_2O data in particular indicate a distinct difference between the groups (Fig. 6f).

Trends of enrichment in K_2O and depletion in Na_2O with increasing SiO_2 in all matrix glasses are consistent with groundmass crystallisation dominated by plagioclase; the main groundmass mineral. K_2O is nearly incompatible in the SHV groundmass assemblage. Thus higher K_2O in dome glasses than pumices has been explained in terms of more extensive groundmass crystallisation (Harford et al. 2003). This interpretation is consistent with groundmass textures: pumice samples contain 20–35% modal glass, whereas dome samples can have as little as 5% modal glass (Murphy et al. 2000; Harford et al. 2003; Couch et al. 2003). While groundmass crystallisation is certainly important, a difficulty with this interpretation arises because matrix glass in dome lavas and pumices with similar SiO_2 contents (i.e. similar amounts of groundmass crystallisation), have very different K_2O contents (Fig. 6). Hornblende breakdown releases K_2O into the host melt, but not enough to account for the observed differences in K_2O content. Complete hornblende breakdown and partitioning of all K_2O into a small fraction of residual melt (~10 wt%) could increase dome melt K_2O contents by no more than 0.15 wt% relative to pumice glasses. Another source of glass composition variability is magma mingling between residual melts from different magma batches (Rutherford and Devine 2003).

Normative compositions for the Soufrière Hills glass compositions have been projected onto the An-corrected ternary system Qz′–Ab′–Or′ using the calculation procedure of Blundy and Cashman (2001). The pumice and dome matrix glasses define contrasting trends (Figs. 7, 8). Pumice glasses (Fig. 7a, b) trend steeply away from Ab′ towards the 0.1 MPa quartz–feldspar cotectic at about Qz′ = 50%, Ab′ = 35% and Or′ = 15%. Dome glasses (Fig. 8a, b) follow a shallow trend away from the Ab′–Qz′ join at about Ab′ = 85% and Qz′ = 15% roughly delineating the eutectic position over a range of decreasing pressures. These respective matrix glass trends extend back to the compositions of melt inclusions in hornblendes and the average groundmass composition estimated by Murphy et al. (2000). The pumice trend is as expected for rapid decompression involving plagioclase crystallisation without reaching the silica phase field (Blundy and Cashman 2001). The high Qz′ content of some pumice glasses indicates partial equilibration at low pressures before quenching by explosive eruption. The dome glasses plot to the Or′-rich side of their pumice counterparts, reflecting higher K_2O contents in the melts. This trend plausibly reflects either physical or chemical mixing between melts ascending at different rates from the magma chamber and experiencing different amounts of groundmass crystallisation en route. We have simulated mixing between melts from different levels by combining compositions of evolved low pressure matrix melts and least evolved melts from inclusions in hornblende at 10% increments. Resulting intermediate melt compositions plot along a similar shallow trend to natural melts in dome samples (Fig. 8a), consistent with the premise that dome glasses are mixtures of melts ascending at different rates.

Hornblende reaction rim glasses

Interstitial glass within hornblende reaction rims is rhyolitic with SiO_2 varying between 69.9 and 80.0 wt% (normalised to 100 wt% anhydrous; Table 10). Compositions are heterogeneous and more variable than matrix glasses (Fig. 6). Notably interstitial reaction rim glasses show the same groupings as the corresponding matrix glasses in terms of K_2O, Na_2O and CaO (Fig. 6) and lie along the corresponding trends in the Qz′–Ab′–Or′ projections (Figs. 7, 8). Other components are more variable with significant heterogeneity within single reaction rims. Some interstitial glass is indistinguishable from surrounding matrix glass whereas other glasses are enriched or depleted in some components. Enrichments in FeO^T and TiO_2 are prominent in many interstitial glasses and a small number of reaction rim glasses are rich in MgO and poor in SiO_2.

Table 9 Interstitial melt compositions in hornblende reaction rims

Sample number	Composition (wt%)									Unnorm total	Qz′	Or′	Ab′
	SiO_2	TiO_2	Al_2O_3	$FeO^{(T)}$	MnO	MgO	CaO	Na_2O	K_2O				
MVO1090B (pumice), rim width = 137 μm	70.63	0.44	15.08	3.13	0.16	1.23	3.76	3.92	1.65	97.80	23.3	6.1	70.5
	72.06	0.32	14.00	3.48	0.11	1.21	2.76	4.10	1.96	96.51	27.8	8.8	63.4
	74.33	0.42	13.73	2.24	b.d.	0.30	3.03	3.95	2.00	97.66	30.1	9.4	60.5
	76.83	0.48	11.77	2.98	0.19	0.25	1.70	3.69	2.12	95.57	38.9	12.1	49.0
	73.46	**0.42**	**13.65**	**2.96**	**0.12**	**0.75**	**2.81**	**3.92**	**1.93**	**96.89**	**30.0**	**9.1**	**60.9**
	2.71	0.07	1.38	0.52	0.08	0.55	0.85	0.17	0.20				
MVO1006w (pumice), rim width = 97 μm	69.85	0.48	15.42	2.20	0.42	1.54	4.39	4.38	1.32	99.09	21.0	4.3	74.6
	72.42	0.64	15.57	1.86	0.19	0.20	4.20	3.31	1.61	98.30	24.3	7.3	68.3
	72.52	0.56	13.72	2.67	0.03	1.65	4.70	2.82	1.33	95.97	25.5	7.6	66.8
	72.67	0.67	14.12	2.98	0.06	1.51	2.64	2.67	2.59	95.91	35.1	14.9	50.0
	73.26	0.50	14.69	3.35	0.37	0.48	2.72	2.49	2.13	98.55	37.2	13.4	49.4
	73.53	0.38	14.77	1.78	0.23	0.18	3.26	4.06	1.82	98.52	27.0	7.7	65.3
	73.87	0.39	14.17	2.13	0.05	0.50	3.35	3.97	1.56	100.02	27.6	7.1	65.3
	73.91	0.76	13.15	3.06	0.43	0.37	2.60	3.61	2.12	98.19	32.4	10.8	56.8
	74.25	0.63	13.82	2.75	0.08	0.39	2.60	3.15	2.33	96.30	34.6	12.7	52.7
	74.38	0.51	14.10	1.87	b.d.	0.36	3.19	3.85	1.73	97.71	28.8	8.0	63.2
	75.52	0.61	12.70	2.38	0.21	0.28	1.47	4.14	2.69	99.77	35.1	14.5	50.5
	76.09	0.94	12.53	2.68	0.03	0.34	2.05	3.06	2.29	96.94	39.7	13.4	46.9
	77.12	0.73	12.07	2.20	0.12	0.26	1.74	3.21	2.55	97.14	40.5	14.6	44.8
	77.71	0.39	11.54	2.31	0.21	0.60	1.93	3.07	2.25	96.57	41.0	13.3	45.8
	74.08	**0.59**	**13.74**	**2.44**	**0.17**	**0.62**	**2.92**	**3.41**	**2.02**	**97.78**	**32.1**	**10.7**	**57.2**
	2.05	0.16	1.21	0.48	0.14	0.53	1.00	0.59	0.46				
MVO177 (dome lava), rim width = 239 μm	73.09	0.32	13.21	3.09	0.18	1.09	1.59	3.18	4.25	98.63	32.1	22.4	45.5
	73.68	0.27	13.11	2.96	b.d.	0.85	1.18	2.42	5.53	98.66	34.0	30.9	35.0
	74.43	0.31	13.58	1.84	0.07	0.02	0.97	3.72	5.06	99.96	30.4	26.8	42.8
	75.00	0.35	13.06	2.28	0.05	0.11	0.64	2.73	5.79	99.28	35.2	33.5	31.3
	75.44	0.23	12.06	2.32	0.41	0.02	0.57	3.06	5.91	99.56	33.7	35.2	31.1
	75.50	0.25	12.43	2.61	0.05	0.08	0.52	2.72	5.84	100.01	35.7	34.4	29.9
	75.68	0.32	12.36	2.00	b.d.	b.d.	0.59	2.98	6.05	100.17	33.6	34.8	31.7
	75.84	0.40	11.99	2.47	0.19	0.34	0.93	2.44	5.40	99.20	37.6	30.9	31.5
	75.93	0.33	12.48	1.98	0.11	0.12	0.61	2.52	5.91	99.07	36.8	34.3	28.9
	76.16	0.35	12.25	2.22	0.22	0.12	0.55	2.38	5.75	98.34	38.8	34.1	27.1
	76.50	0.37	12.18	2.23	0.18	0.11	0.66	2.20	5.57	98.20	40.5	33.0	26.5
	76.66	0.19	12.12	2.02	0.09	0.08	0.39	2.59	5.86	99.25	38.1	34.9	27.1
	76.69	0.14	11.88	2.66	0.04	0.18	0.67	2.46	5.27	100.24	39.9	31.2	28.9
	76.71	0.51	11.59	2.32	0.27	0.16	0.41	2.44	5.58	100.52	40.2	33.7	26.1
	76.90	0.30	11.71	2.19	b.d.	0.05	0.59	2.55	5.71	100.01	38.2	33.2	28.6
	77.67	0.34	11.50	1.93	0.09	0.11	0.68	2.59	5.10	98.76	40.7	29.7	29.6
	75.74	**0.31**	**12.34**	**2.32**	**0.12**	**0.22**	**0.72**	**2.69**	**5.54**	**99.37**	**36.6**	**32.1**	**31.3**
	1.22	0.09	0.61	0.36	0.11	0.31	0.31	0.38	0.45				
MVO1217 (dome lava) Phenocryst 2, rim width = 105 μm	73.25	0.52	13.12	4.35	b.d.	0.04	2.08	2.98	3.66	100.18	33.8	19.0	47.2
	74.15	0.44	13.16	1.65	b.d.	0.58	1.92	4.71	3.37	99.76	29.8	18.4	51.8
	74.73	0.34	13.21	1.77	b.d.	0.03	2.03	4.39	3.49	99.33	31.2	18.3	50.5
	75.11	0.72	12.25	1.82	0.20	0.78	1.46	2.15	5.51	97.42	35.7	29.7	34.6
	75.82	0.82	12.09	1.42	0.20	0.55	0.94	2.16	5.99	99.37	37.0	33.7	29.2
	76.05	0.75	11.53	1.12	b.d.	0.04	0.61	2.80	7.10	99.39	35.3	44.0	20.7
	77.29	0.71	12.65	0.59	0.06	0.06	1.07	2.38	5.19	97.41	39.9	28.9	31.3
	77.87	0.76	11.79	1.02	b.d.	0.03	0.23	2.11	6.20	97.84	42.1	37.1	20.8
	78.06	0.66	11.55	0.95	0.06	0.27	0.70	2.08	5.68	97.72	41.9	32.9	25.3
	78.31	0.38	11.48	0.71	0.22	0.06	0.30	2.43	6.12	98.10	39.9	35.9	24.2
	78.41	0.58	11.66	0.86	b.d.	0.17	0.29	2.10	5.94	97.72	43.2	35.5	21.3
	78.76	0.58	11.39	0.72	b.d.	b.d.	0.78	2.26	5.52	97.66	41.6	31.2	27.2
	79.34	0.60	11.36	0.62	0.03	0.08	0.16	2.10	5.72	97.92	45.7	34.4	19.9
	76.70	**0.60**	**12.10**	**1.35**	**0.06**	**0.21**	**0.97**	**2.67**	**5.35**	**98.45**	**38.2**	**30.7**	**31.1**
	1.96	0.15	0.71	1.00	0.09	0.26	0.70	0.88	1.14				
Phenocryst 5, rim width = 49 μm	71.05	0.44	17.35	0.18	0.10	0.06	4.18	3.57	3.08	98.33	22.5	7.8	69.7
	71.35	0.21	16.79	0.73	b.d.	0.05	3.68	4.15	3.04	100.21	22.3	7.7	70.0
	73.19	0.59	15.21	0.95	0.07	0.11	1.73	4.18	3.96	100.37	28.4	18.2	53.4
	74.29	0.13	15.04	0.52	0.12	b.d.	1.59	2.86	5.46	99.63	31.6	26.6	41.7
	76.29	0.83	13.07	1.23	b.d.	0.03	0.34	2.10	6.11	96.75	41.0	36.8	22.2
	76.56	0.60	12.55	1.39	b.d.	0.62	1.50	2.52	4.26	96.76	39.4	23.8	36.7
	76.61	0.61	13.16	0.86	b.d.	0.13	0.22	2.31	6.10	96.76	40.4	36.9	22.7
	77.16	0.92	12.71	0.75	0.04	0.13	0.18	2.16	5.96	97.97	42.7	36.3	21.0
	77.18	0.98	12.52	0.85	0.12	0.17	0.83	2.75	4.59	96.82	41.3	26.5	32.2
	77.24	0.38	13.13	0.67	0.10	b.d.	1.53	2.76	4.17	96.36	39.0	22.6	38.4
	77.37	0.80	12.92	0.81	b.d.	0.07	0.44	2.01	5.58	96.14	44.2	33.5	22.2

Table 9 (Contd.)

78.36	0.95	11.65	1.57	0.19	b.d.	0.36	1.73	5.19	96.51	48.9	32.0	19.0	
79.30	1.08	11.25	0.69	b.d.	0.06	0.38	1.99	5.24	97.00	47.4	31.5	21.1	
75.84	**0.66**	**13.64**	**0.86**	**0.06**	**0.11**	**1.30**	**2.70**	**4.83**	**97.66**	**37.6**	**26.2**	**36.2**	
2.58	0.30	1.88	0.06	0.06	0.16	1.30	0.81	1.07					
Phenocryst 6,	75.62	b.d.	13.25	0.65	0.04	b.d.	0.21	2.56	7.66	99.89	30.8	44.6	24.7
rim width = 253 μm	75.92	0.82	13.58	0.51	0.02	b.d.	0.19	2.63	6.32	97.48	37.0	37.9	25.1
	77.37	0.69	12.92	0.62	0.12	b.d.	1.01	2.45	4.81	95.17	41.5	27.3	31.2
	77.56	0.71	12.65	0.83	0.22	b.d.	0.78	2.59	4.65	96.26	42.6	27.1	30.3
	78.36	0.48	11.88	0.54	0.05	0.02	0.29	2.32	6.06	96.81	41.3	35.7	23.1
	78.49	0.69	11.72	0.59	0.11	0.04	0.39	2.01	5.97	97.12	43.3	35.2	21.5
	78.79	0.83	12.21	0.41	0.14	0.06	0.18	1.87	5.50	96.99	48.0	33.7	18.3
	78.80	0.61	11.54	0.55	0.04	0.05	0.74	2.14	5.53	94.66	42.5	31.6	25.8
	79.78	0.36	10.78	0.54	0.09	0.07	0.64	2.55	5.19	98.43	43.0	29.9	27.1
	80.03	0.60	10.64	0.88	b.d.	b.d.	0.45	2.33	5.07	97.70	45.7	29.8	24.5
	78.07	**0.58**	**12.12**	**0.61**	**0.08**	**0.03**	**0.49**	**2.35**	**5.68**	**97.05**	**41.6**	**33.3**	**25.1**
	1.47	0.25	0.99	0.14	0.07	0.03	0.29	0.26	0.88				

All compositions are normalised to 100% anhydrous for comparison. Totals are unnormalised. Each composition is a single analysis. Compositions in bold type are averages of the reported data for each sample; figures in italics indicate one standard deviation of the average compositions
b.d. below detection

Table 10 Matrix glass compositions in the recent Soufrière Hills Volcano andesite

Sample number	Composition (wt%)									Unnorm total	Qz′	Or′	Ab′
	SiO_2	TiO_2	Al_2O_3	$FeO^{(T)}$	MnO	MgO	CaO	Na_2O	K_2O				
MVO1090B (pumice)	74.85	0.34	14.06	1.33	b.d.	0.24	3.09	4.24	1.85	94.95	29.2	8.3	62.4
	75.63	0.42	13.13	1.35	0.15	0.31	2.62	4.31	2.08	93.40	32.6	10.4	57.0
	76.07	0.29	13.11	1.63	b.d.	0.30	2.21	4.35	2.04	96.28	32.9	10.2	56.9
	77.10	0.47	12.25	1.74	b.d.	0.41	1.99	3.79	2.25	96.39	36.6	12.0	51.4
	77.22	0.32	11.96	1.80	b.d.	0.31	1.92	4.24	2.18	93.45	37.2	12.0	51.4
	77.33	0.30	11.78	1.93	b.d.	0.40	2.01	3.97	2.28	95.50	37.9	12.6	50.8
	77.42	0.36	11.56	1.81	0.12	0.46	2.17	3.94	2.15	95.79	38.6	12.1	49.3
	77.85	0.37	11.69	1.81	0.07	0.36	1.76	4.00	2.08	96.00	38.6	11.5	49.9
	76.68	**0.36**	**12.44**	**1.68**	**0.05**	**0.35**	**2.22**	**4.11**	**2.11**	**95.22**	**35.5**	**11.1**	**53.4**
	1.04	0.06	0.89	0.22	0.06	0.07	0.43	0.21	0.14				
MVO1006w (pumice)	72.03	0.31	15.75	1.46	b.d.	0.09	4.08	4.62	1.66	98.92	22.7	5.5	71.7
	72.14	0.31	15.95	1.08	0.23	0.11	3.87	4.63	1.67	99.60	22.4	5.4	72.3
	72.17	0.30	15.57	1.43	0.27	0.30	4.11	4.16	1.69	98.79	23.2	5.9	70.9
	72.32	0.24	15.86	1.23	b.d.	0.12	4.24	4.42	1.57	98.95	22.3	5.2	72.5
	73.30	0.51	14.29	2.08	0.08	0.64	3.15	4.05	1.90	96.94	27.7	8.3	64.0
	73.73	0.37	13.83	2.22	0.07	0.58	3.13	4.28	1.79	97.75	29.0	8.3	62.8
	75.00	0.31	14.07	1.71	0.12	0.23	2.90	3.75	1.90	97.27	31.0	9.3	59.7
	75.82	0.37	13.41	1.49	0.17	0.11	2.41	4.10	2.12	96.60	32.2	10.2	57.6
	77.50	0.35	12.12	1.59	0.16	0.20	2.14	3.82	2.12	97.30	37.1	11.4	51.5
	78.84	0.41	11.37	1.54	0.07	0.15	1.57	3.76	2.29	97.49	40.6	12.8	46.6
	74.29	**0.35**	**14.22**	**1.58**	**0.12**	**0.25**	**3.16**	**4.16**	**1.87**	**97.96**	**28.8**	**8.2**	**63.0**
	2.43	0.01	1.61	0.35	0.09	0.20	0.92	0.33	0.24				
MVO177 (dome lava)	73.10	0.35	14.61	1.26	b.d.	0.08	2.24	3.93	4.38	99.39	27.3	19.3	53.4
	74.09	0.25	13.88	1.51	0.08	0.10	2.07	3.49	4.53	99.28	30.1	21.3	48.6
	75.24	0.13	12.93	1.46	0.07	0.06	1.49	3.57	5.06	98.96	31.9	27.6	40.5
	75.47	0.21	13.29	0.99	b.d.	0.07	2.20	3.97	3.79	98.87	32.2	19.1	48.7
	76.41	0.40	11.97	1.53	0.15	0.10	1.00	3.25	5.19	98.45	35.7	30.0	34.3
	77.21	0.38	11.48	1.37	0.05	0.04	0.78	3.18	5.50	98.90	37.1	33.2	29.7
	75.25	**0.29**	**13.03**	**1.35**	**0.07**	**0.07**	**1.63**	**3.56**	**4.74**	**98.98**	**32.4**	**25.1**	**42.5**
	1.37	0.10	1.07	0.19	0.04	0.02	0.58	0.30	0.57				
MVO1217 (dome lava)	75.86	0.56	13.21	0.57	0.11	b.d.	1.53	3.10	4.87	95.06	33.8	24.3	41.9
	78.77	0.94	10.87	1.06	0.06	0.25	0.61	2.15	5.34	98.90	43.9	31.3	24.8
	79.95	0.45	10.26	0.52	0.30	b.d.	0.68	2.25	5.58	98.73	44.6	33.1	22.3
	80.02	0.67	10.82	0.80	b.d.	0.02	0.36	2.13	5.22	100.47	47.0	31.0	22.0
	80.09	0.64	10.63	0.75	0.08	b.d.	0.68	2.11	5.09	98.64	45.7	29.5	24.7
	81.11	0.48	10.42	0.49	b.d.	0.08	0.18	1.95	5.29	97.57	49.6	31.7	18.6
	79.30	**0.62**	**11.04**	**0.70**	**0.09**	**0.06**	**0.67**	**2.28**	**5.23**	**98.23**	**44.1**	**30.2**	**25.7**
	1.84	0.18	1.09	0.22	0.11	0.10	0.47	0.41	0.24				

All compositions are normalised to 100% anhydrous for comparison. Each composition is a single analysis. Compositions in bold type are averages of the reported data for each sample; figures in italics indicate one standard deviation on the average compositions *b.d.* below detection.

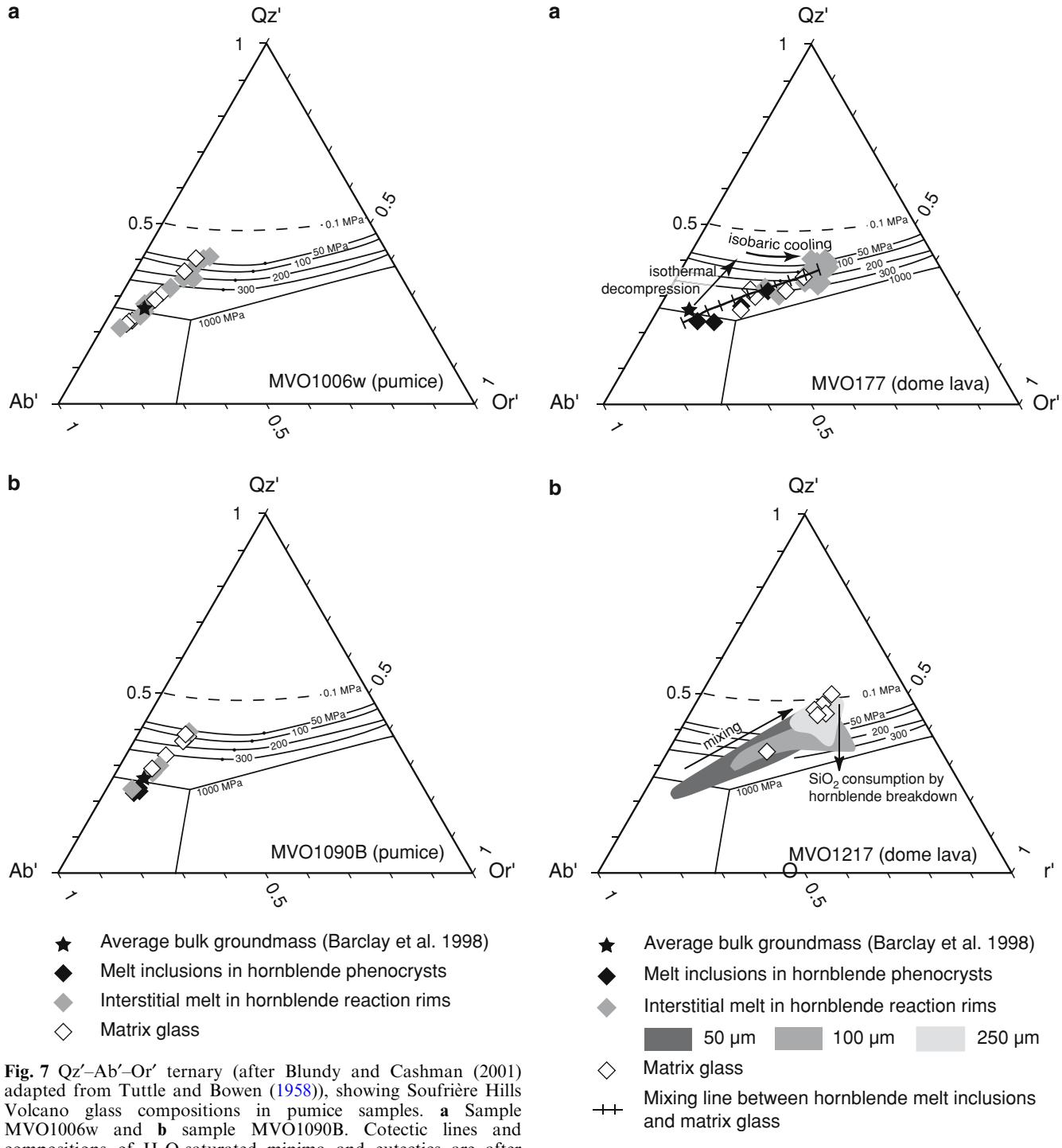

Fig. 7 Qz′–Ab′–Or′ ternary (after Blundy and Cashman (2001) adapted from Tuttle and Bowen (1958)), showing Soufrière Hills Volcano glass compositions in pumice samples. **a** Sample MVO1006w and **b** sample MVO1090B. Cotectic lines and compositions of H_2O-saturated minima and eutectics are after Blundy and Cashman (2001) for a range of water pressures. Neither sample contains a silica phase; consequently cotectics corresponding to the positions of these glasses give maximum rather than actual P_{H_2O} conditions of melt equilibration

Fig. 8 Qz′–Ab′–Or′ ternary showing Soufrière Hills Volcano glass compositions in lava dome samples. **a** Sample MVO177. The *mixing line* shows the range of melt compositions that could be achieved by mixing the least evolved melt inclusion material with the most evolved matrix glass. *Plot symbols* mark increments of 10% in melt proportions. **b** Sample MVO1217. Silica microlites are present in both the matrix glass and interstitial reaction rim melt (*thick rim*). This allows quantitative estimates of the pressures at which these melts were last equilibrated (100 to <25 MPa for the matrix and <100 MPa for reaction rim melt). Scatter in Qz′ values (*vertical arrows*) in interstitial reaction rim melts might result from SiO_2 consumption from the melt during hornblende dehydration

We have already shown that hornblende breakdown requires an open system with exchanges of components with the surrounding melt. Some of the interstitial glasses within reaction rims are similar to the host matrix glass and can be interpreted as surrounding melt

infiltrating the reaction rims. In there cases the interstitial reaction rim glass faithfully mirrors the matrix glass (Figs. 6, 7, 8). However, other glasses are markedly different and are mostly consistent with the chemical exchanges suggested by the mass balance calculations. In particular the calculations infer releases of TiO_2 and MgO into the melt, which can explain the interstitial glasses enriched in these elements. Exchanges in SiO_2 and Na_2O are more difficult to interpret since these elements vary considerably in matrix glasses, due to variable groundmass crystallisation. FeO^T is the only discrepancy, being consumed in reaction 2a, but enriched in many interstitial glasses relative to the matrix glasses.

Conclusions

Hornblende phenocrysts in recent Soufrière Hills Volcano andesites display reaction rims of microcrystalline plagioclase, pyroxene, Fe-oxides and interstitial glass, formed by hornblende dehydration during magma ascent and decompression. Mass balance calculations give the following reactions, with mineral proportions in agreement with modal abundances expressed as mass fractions:

$$100.0\text{hbl} \rightarrow 49.8\text{cpx} + 27.6\text{opx} + 18.2\text{plag} + 4.5\text{Ti-mag}$$
$$100.0\text{hbl} \rightarrow 53.9\text{cpx} + 24.4\text{opx} + 18.1\text{plag} + 1.9\text{ilm} + 1.7\text{mag}$$

Re-evaluation of the compositional data and material balance estimates for hornblende breakdown in post May 18, 1980, MSH andesites (Rutherford and Hill 1993) gives the reaction:

$$100.0\,\text{hbl} \rightarrow 43.0\,\text{cpx} + 24.5\,\text{opx} + 23.7\,\text{plag} + 5.2\,\text{mag} + 3.5\,\text{ilm}$$

Both MSH and Soufrière Hills Volcano hornblende dehydration reactions occurred in open chemical systems with exchange of most components between the hornblende and the melt. The reactions studied reveal deficiencies in SiO_2 and Fe-oxides, and excesses of Na_2O and K_2O, the residuals presumably being accommodated by the surrounding melt. Volatiles (H_2O and Cl) must also be released by the reaction. These results imply that transport of mobile components in the melt must play a part in rim growth. It follows that transport processes may have the potential to control the rate of reaction rim growth.

Matrix glasses fall into two compositional groups. Glasses in pumice are relatively rich in CaO and poor in K_2O and Na_2O compared to glasses in dome samples. The former glasses formed by moderate amounts of groundmass crystallisation of plagioclase associated with rapid magma ascent in explosive eruptions. The latter glasses reflect mixing between melts that experienced extensive groundmass crystallisation and hornblende breakdown during slow magma ascent and extended residence time in the dome, and less evolved melts that ascended more rapidly from the magma chamber. Interstitial glass compositions in hornblende reaction rims reflect the compositions of the surrounding matrix glasses, but show variable compositional differences mostly consistent with the proposed open-system hornblende breakdown reactions.

Acknowledgements This work benefited from helpful discussions with Jon Blundy, Alison Pawley and Tim Elliott. Stuart Kearns, Chloe Harford, Nicola Steen and Bruce Paterson are thanked for providing helpful analytical advice. We are also grateful to Mick Murphy for contributing photomicrographs from his collection (Fig. 1a–d), and to the *Journal of Petrology* for permitting us to reproduce Fig. 1d. The assistance of MVO staff and associates in obtaining the samples used in this study is gratefully acknowledged. V.J.E.B. acknowledges a Natural Environmental Research Council studentship and R.S.J.S support from a Royal Society Wolfson Merit Award. The manuscript was improved by the helpful reviews of Malcolm Rutherford and Mike Carroll.

References

Blundy J, Cashman K (2001) Ascent-driven crystallisation of dacite magmas at Mount St Helens, 1980–1986. Contrib Mineral Petrol 140:631–650 (DOI 10.1007/s004100000219)

Candela PA (1986) The evolution of aqueous vapor from silicate melts: effect on oxygen fugacity. Geochim Cosmochim Acta 50:1205–1211

Clynne MA (1999) A complex magma mixing origin for rocks erupted in 1915, Lassen Peak, California. J Petrol 40:105–132

Conte AM (1993) High temperature breakdown in calcalkaline subvolcanic rocks from Sarroch District (Sardinia, Italy): implications for mixing processes. N Jahrb Mineral Monatsh 3:133–144

Couch S, Sparks RSJ, Carroll MR (2001) Mineral disequilibrium in lavas explained by convective self-mixing in open magma chambers. Nature 411:1037–1039

Couch S, Harford CL, Sparks RSJ, Carroll MR (2003) Experimental constraints on the conditions of formation of highly calcic plagioclase microlites at the Soufrière Hills Volcano, Montserrat. J Petrol 44:1455–1475

Devine JD, Gardner JE, Brack HP, Layne GD, Rutherford MJ (1995) Comparison of microanalytical methods for estimation of H_2O contents of silicic volcanic glasses. Am Mineral 80:319–328

Devine JD, Murphy MD, Rutherford MJ, Barclay J, Sparks RSJ, Carroll MR, Young SR, Gardner JE (1998a) Petrologic evidence for pre-eruptive pressure–temperature conditions, and recent reheating, of andesitic magma erupting at the Soufrière Hills Volcano, Montserrat, WI. Geophys Res Lett 25:3669–3672

Devine JD, Rutherford MJ, Gardner JE (1998b) Petrologic determination of ascent rates for the 1995–1997 Soufrière Hills Volcano andesitic magma. Geophys Res Lett 25:3673–3676

Devine JD, Rutherford MJ, Norton GE, Young SR (2003) Magma storage region processes inferred from geochemistry of Fe–Ti oxides in andesitic magma, Soufrière Hills Volcano, Montserrat, WI. J Petrol 44:1375–1400

Droop GTR (1987) A general equation for estimating Fe^{3+} concentrations in ferromagnesian silicates and oxides from microprobe analyses, using stoichiometric criteria. Mineral Mag 51:431–435

Garcia MO, Jacobson SS (1979) Crystal clots, amphibole fractionation and the evolution of calc-alkaline magmas. Contrib Mineral Petrol 69:319–327

Gust DA, Johnson RW (1981) Amphibole bearing inclusions from Boisa Island, Papua New Guinea: evaluation of the role of fractional crystallisation in an andesitic volcano. J Geol 89:219–232

Harford CL, Pringle MS, Sparks RSJ, Young SR (2002) The volcanic evolution of Montserrat using $^{40}Ar/^{39}Ar$ geochronology. In: Druitt TH, Kokelaar BP (eds) The eruption of Soufrière Hills Volcano, Montserrat, from 1995 to 1999. Geol Soc Lond Mem 21:93–113

Harford CL, Sparks RSJ, Fallick AE (2003) Degassing at the Soufrière Hills Volcano, Montserrat, recorded in matrix glass compositions. J Petrol 44:1503–1523

Jakes P, White AJR (1972) Hornblendes from calc-alkaline volcanic rocks of island arcs and continental margins. Am Mineral 57:887–902

Leake BE, Woolley AR, Arps CES, Birch WD, Gilbert MC, Grice JD, Hawthorne FC, Kato A, Kisch HJ, Krivovichev VG, Linthout K, Laird J, Mandarino J, Maresch WV, Nickel EH, Rock NMS, Schumacher JC, Smith DC, Stephenson NCN, Ungaretti L, Whittaker EJW, Youzhi G (1997) Nomenclature of amphiboles: Report of the Subcommittee on Amphiboles of the International Mineralogical Association Commission on New Minerals and Mineral Names. Mineral Mag 61:295–321

Morgan GB, London D (1996) Optimizing the electron microprobe analysis of hydrous alkali aluminosilicate glasses. Am Mineral 81:1176–1185

Murphy MD, Sparks RSJ, Barclay J, Carroll MR, Lejeune AM, Brewer TS, Macdonald R, Black S, Young S (1998) The role of magma mixing in triggering the current eruption at the Soufrière Hills volcano, Montserrat, West Indies. Geophys Res Lett 25:3433–3436

Murphy MD, Sparks RSJ, Barclay J, Carroll MR, Brewer TS (2000) Remobilization of andesite magma by intrusion of mafic magma at the Soufrière Hills Volcano, Montserrat, West Indies. J Petrol 41:21–42

Pouchou JL, Pichoir F (1985) "PAP" (ϕ–ρ– z) correction procedure for improved quantitative microanalysis. In: Armstrong JT (ed) Microbeam analysis. San Francisco Press, San Francisco CA, pp 104–106

Reagan MK, Gill JB, Malavassi E, Garcia MO (1987) Changes in magma composition at Arenal volcano, Costa Rica, 1968–1985: real-time monitoring of open-system differentiation. Bull Volcanol 49:415–434

Robertson REA, Aspinall WP, Herd RA, Norton GE, Sparks RSJ, Young SR (2000) The 1995–1998 eruption of the Soufrière Hills volcano, Montserrat, WI. Phil Trans R Soc Lond Ser A 358:1619–1637

Roobol MJ, Smith AL (1998) Pyroclastic stratigraphy of the Soufrière Hills volcano, Montserrat: implications for the present eruption. Geophys Res Lett 25:3393–3396

Rutherford MJ, Devine JD (2003) Magmatic conditions and magma ascent as indicated by hornblende phase equilibria and reactions in the 1995–2002 Soufrière Hills magma. J Petrol 44:1433–1454

Rutherford MJ, Hill PM (1993) Magma ascent rates from amphibole breakdown: an experimental study applied to the 1980–1986 Mount St. Helens eruptions. J Geophys Res 98:19667–19685

Scarfe CM, Fuji T (1987) Petrology of crystal clots in the pumice of Mount St. Helens' March 19, 1982 eruption; significant role of Fe–Ti oxide crystallisation. J Volcanol Geotherm Res 34:1–14

Schmidt RG (1957) Petrology of the volcanic rocks, Saipan, Mariana Islands. US Geol Surv Prof Pap 280:127–176

Sparks RSJ, Young SR, Barclay J, Calder ES, Cole P, Darroux B, Davies MA, Druitt TH, Harford C, Herd R, James M, Lejeune AM, Loughlin S, Norton G, Skerrit G, Stasiuk MV, Stevens NS, Toothill J, Wadge G, Watts R (1998) Magma production and growth of the lava dome of the Soufrière Hills Volcano, Montserrat, West Indies: November 1995 to December 1997. Geophys Res Lett 25:3421–3424

Tuttle OF, Bowen NL (1958) Origin of granite in the light of experimental studies in the system $NaAlSi_3O_8$–$KAlSi_3O_8$–SiO_2–H_2O. Geological Society of America Memoir 74, Boulder, CO, 153 p

Williams H (1942) The geology of Crater Lake National Park, Oregon. Publications of the Carnegie Institute, Washington, DC 540, 162 p

Wright TL, Doherty PC (1970) A linear programming and least squares computer method for solving petrologic mixing problems. Geol Soc Am Bull 81:1995–2008